

## Quantifying seasonal bias in street view imagery for urban form assessment: A global analysis of 40 cities

Tianhong Zhao<sup>a</sup>, Xiucheng Liang<sup>b</sup>, Filip Biljecki<sup>b,c</sup>, Wei Tu<sup>d</sup>, Jinzhou Cao<sup>a,\*\*</sup>, Xiaojiang Li<sup>e</sup>, Shengao Yi<sup>e,f,\*</sup>

<sup>a</sup> College of Big Data and Internet, Shenzhen Technology University, Shenzhen 518118, China

<sup>b</sup> Department of Architecture, National University of Singapore, Singapore 117566, Singapore

<sup>c</sup> Department of Real Estate, National University of Singapore, Singapore 119077, Singapore

<sup>d</sup> Shenzhen Key Laboratory of Spatial Information Smart Sensing and Services, Department of Urban Informatics, School of Architecture and Urban Planning, Shenzhen University, Shenzhen 518060, China

<sup>e</sup> Department of City and Regional Planning, University of Pennsylvania, Philadelphia, PA 19104, USA

<sup>f</sup> Penn Institute for Urban Research, University of Pennsylvania, Philadelphia, PA 19104, USA

### ARTICLE INFO

#### Keywords:

Google street view

Urban sensing

GeoAI

Data quality

Consistency

### ABSTRACT

Street view imagery (SVI), with its rich visual information, is increasingly recognized as a valuable data source for urban research. Particularly, by leveraging computer vision techniques, SVI can be used to calculate various urban form indices (e.g., Green View Index, GVI), providing a new approach for large-scale quantitative assessments of urban environments. However, SVI data collected at the same location in different seasons can yield varying urban form indices due to phenological changes, even when the urban form remains constant. Numerous studies overlook this kind of seasonal bias. To address this gap, we propose a systematic analytical framework for quantifying and evaluating seasonal bias in SVI, drawing on more than 262,000 images from 40 cities worldwide. This framework encompasses three aspects: seasonal bias within urban areas, seasonal bias across cities on a global scale, and the impact of seasonal bias in practical applications. The results reveal that (1) seasonal bias is evident, with an average mean absolute percentage error (MAPE) of 54 % for GVI across all sampled cities, and it is particularly pronounced in areas with significant seasonal bias; (2) seasonal bias is strongly correlated with geographic location, with greater bias observed in cities with lower average rainfall and temperatures; and (3) in practical applications, ignoring seasonal bias may result in analytical errors (e.g., an ARI of 0.35 in clustering). By identifying and quantifying seasonal bias in SVI, this study contributes to improving the accuracy of urban environmental assessments based on street view data and provides new theoretical support for the broader application of such data on a global scale.

### 1. Introduction

Street View Imagery (SVI) data, as an emerging data source, provides rich urban visual information and has become a significant tool in urban environmental research (Biljecki & Ito, 2021). SVI data are typically captured using cameras installed on vehicles or carried by pedestrians, recording detailed landscape information along urban streets. Compared to traditional remote sensing images and geographic information data, SVI data offer higher resolution and a more realistic ground-level perspective, enabling the capture of more detailed urban environmental features (Kang et al., 2021; Zhang, Wu, Zhu, & Liu, 2019). In

recent years, the application of SVI has attracted a great deal of attention in various fields such as urban planning, traffic management, and environmental monitoring (Wang et al., 2024; Yao et al., 2021; Zhang, Zhang, Fang, & Chen, 2023). Through computer vision techniques, such as semantic segmentation, multiple urban environmental indicators can be extracted from SVI, including Sky View Factor (SVF), Green View Index (GVI), and Building View Index (BVI) (Biljecki, Zhao, Liang, & Hou, 2023; Gong et al., 2018). These indicators not only help urban planners and policymakers better understand the urban environment but are also used to analyze urban microclimates, optimize public space design (Dong et al., 2025), and improve the quality of life of urban

\* Corresponding author at: Department of City and Regional Planning, University of Pennsylvania, Philadelphia, PA 19104, USA.

\*\* Corresponding author at: College of Big Data and Internet, Shenzhen Technology University, Shenzhen 518118, China.

E-mail addresses: [caojinzhou@sztu.edu.cn](mailto:caojinzhou@sztu.edu.cn) (J. Cao), [shengao@upenn.edu](mailto:shengao@upenn.edu) (S. Yi).

residents.

SVI data come from various sources, with bias in data collection methods, equipment types, and spatial and temporal sampling intervals. These differences can lead to substantially different results when the same research questions are addressed using different data strategies (Ito, Kang, Zhang, Zhang, & Biljecki, 2024; Kim & Jang, 2023; Kim, Lee, Hipp, & Ki, 2021). This is especially important considering the rise of crowdsourced SVI, which amplifies the heterogeneity of the data (Helbich, Danish, Labib, & Ricker, 2024; Hou et al., 2024; Juhasz & Hochmair, 2016; Mahabir, Schuchard, Crooks, Croitoru, & Stefanidis, 2020). As SVI data usage in urban studies continues to grow, the bias introduced by the use of different data strategies has received increasing attention (Fan, Feng, & Biljecki, 2025). For example, Biljecki et al. (2023) analyzed how different shooting angles might lead to significant visual discrepancies in SVI of the same location. In addition, bias in camera equipment can cause data differences. Panoramic cameras can capture 360-degree images, offering a more comprehensive view, whereas standard cameras typically capture images in a single direction. The research by Kim et al. (2021) demonstrated that the use of different spatial sampling intervals can also affect the results of the analysis. For example, sampling at 10-m intervals versus 50-m intervals can result in significant differences in data coverage and detail. The presence of dynamic elements in SVIs, such as pedestrians, vehicles, and weather conditions, can also impact the consistency of the data and the stability of the analyses (Hou & Biljecki, 2022).

However, current research rarely evaluates the seasonal bias in the SVI data. Seasonal bias in this study refers to the discrepancies in street-level urban form indicators (e.g., GVI, BVI, SVF) that arise solely from the season of image acquisition, rather than from any actual changes in the built environment. As illustrated in Fig. 1, the difference in vegetation cover between winter and summer is substantial, with vegetation potentially in a withered state during winter and flourishing in summer. Although SVIs are taken from the same location and angle, the GVI and other urban form indicators calculated using semantic segmentation can vary greatly (e.g., the GVI decreases from 0.379 to 0.223, a 41 % decrease), affecting downstream analyzes. Current research not only overlooks the timing of data collection, but also frequently mixes SVI data collected at different times in a city. Such combinations can lead to varying results, a phenomenon this study describes as seasonal bias in SVI. However, to our knowledge, no study has systematically evaluated and quantified the seasonal bias resulting from the different times of SVI data collection. Therefore, the primary objective of this study is to analyze and quantify seasonal bias in SVI data and explore the spatial distribution patterns of this bias. Through this research, our aim is to address the following research questions (RQ).

**RQ1.** How significant is the seasonal bias in the SVI data, and what is its spatial distribution?

**RQ2.** How is the distribution of seasonal bias correlated with climate on a global scale?

**RQ3.** In practical applications, how significant are the errors in analysis results caused by seasonal bias?

This study proposes a comprehensive framework to systematically analyze seasonal bias of SVI in global cities. We begin by introducing a conceptual model that explains how climatic and geographic factors contribute to seasonal variation in urban form indicators derived from SVI. Using a dataset of 262,988 seasonally tagged SVIs from 40 cities worldwide, semantic segmentation techniques were applied to extract three key indicators of urban form: GVI, BVI, and SVF. Seasonal bias is quantified using three metrics: mean absolute error (MAE), mean absolute percentage error (MAPE), and Pearson's correlation coefficient ( $R$ ), enabling a robust assessment of seasonal bias both within cities and between regions. To further investigate global patterns, a standardized index  $B_X$  is constructed to represent the seasonal bias for each urban form indicator at the city level. Ordinary least squares (OLS) regression

is then used to identify how seasonal bias in GVI is shaped by climatic variables such as mean temperature, rainfall, and their intraannual variability. Finally, the study demonstrates the real-world implications of seasonal bias through a functional urban clustering task, showing how variations in data collection season can significantly affect clustering outcomes and introduce bias into urban analysis and decision making.

The primary contributions of this study are as follows: (1) We introduce a systematic framework to quantify seasonal bias in urban form indicators derived from street-level imagery. To our knowledge, this is the first one to establish a framework to quantitatively analyze seasonal bias in SVI and could be generalizable to other types of bias in SVI. (2) We examine seasonal bias in 40 global cities, elucidating the role of climatic and geographic drivers. Our findings reveal how latitude, temperature fluctuations, and rainfall patterns influence the reliability of SVI-based measurements, offering valuable insights for urban perception studies, walkability audits, and greenery assessments. (3) By mapping bias patterns and examining how these biases affect tasks such as functional zoning, we demonstrate that unaccounted for seasonal effects can lead to significant analytical errors. Our results underscore the importance of incorporating seasonal considerations in both the collection and interpretation of SVI for improved precision and reliability in urban research. In general, these contributions promote a deeper understanding of how seasonality can affect SVI, thus forming a variety of research domains, including urban perception, greenery auditing, and walkability, where robust and unbiased SVI-based metrics are vital to evidence-based planning and decision making.

## 2. Related work

### 2.1. SVI in urban research

SVI encompasses rich and detailed visual information on urban environments. These data are typically collected on mobile platforms equipped with panoramic cameras, such as vehicles, backpacks, and drones, to capture comprehensive, high-resolution cityscapes (Biljecki & Ito, 2021; Xue et al., 2021). Compared to traditional remote sensing imagery and aerial photography, the unique advantages of SVI lie in its high resolution and distinctive perspective. Firstly, the high-resolution images provided by SVI enable a detailed analysis of urban microstructures (Cao et al., 2023; Zeng, Lu, Li, & Li, 2018). For example, information on building density, urban layout, street width and pedestrian activity can be obtained accurately, which is crucial for the management and optimization of urban infrastructure (Chen et al., 2024; Dong et al., 2024; Kang, Körner, Wang, Taubenböck, & Zhu, 2018; Li et al., 2022; Ma, Zhang, Yi, & Lu, 2025; Tu et al., 2024). This level of detail surpasses that offered by conventional remote sensing methods, allowing for more precise urban planning and management. Furthermore, the perspective of SVI is closer to ground level, meaning that it captures scenes that are more akin to human visual experience (Cheng et al., 2017; He, Zhang, Yao, & Li, 2023; Luo, Liu, Xu, Zhao, & Biljecki, 2025; Ye, Zeng, Shen, Zhang, & Lu, 2019). This ground-level perspective makes the data more intuitive and easier to interpret while also providing a more accurate reflection of street-level environmental features. Consequently, SVI not only enhances the granularity of urban environmental assessments, but also improves the reliability of data for practical urban planning and management applications (Kruse, Kang, Liu, Zhang, & Gao, 2021; Yao et al., 2021).

The acquisition of SVI typically relies on two primary sources: commercial map service providers and crowdsourced mapping platforms (Kang, Zhang, Gao, Lin, & Liu, 2020). Commercial map service providers, such as Google Street View<sup>1</sup> and Baidu Map,<sup>2</sup> collect data using specialized equipment (e.g. 360-degree panoramic cameras)

<sup>1</sup> <https://www.google.com/maps>

<sup>2</sup> <https://map.baidu.com/>

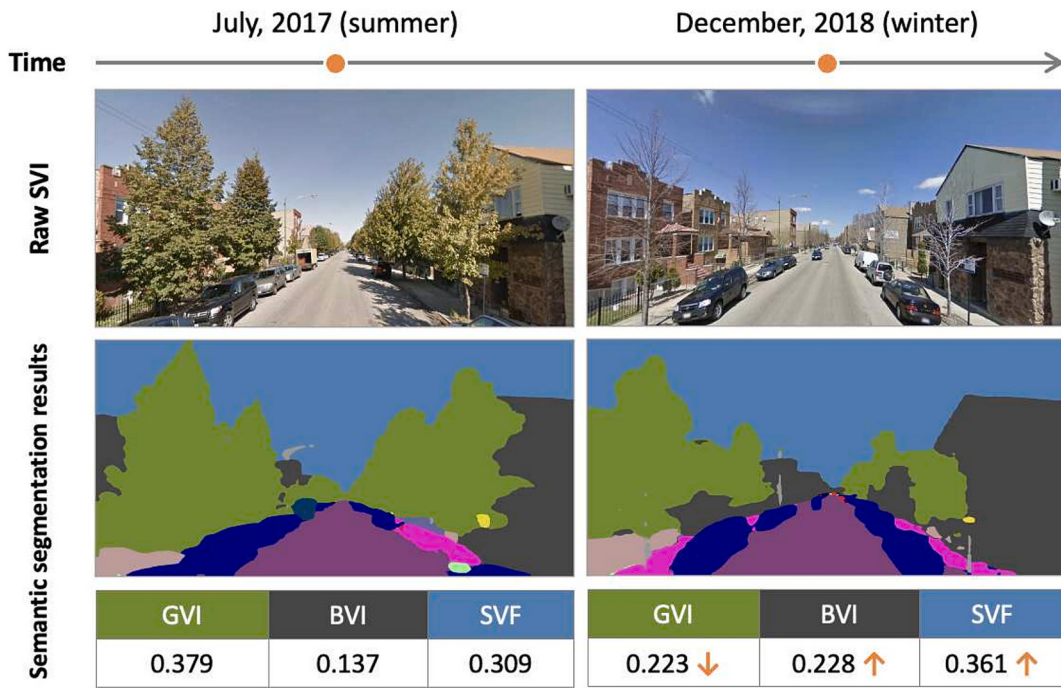


**Fig. 1.** Examples of bias in urban form indicators derived from SVI across different seasons at the same location. Different seasons significantly impact the computation of the GVI, which in turn also affects important metrics such as SVF and BVI.

mounted on vehicles that traverse urban roads, regularly updating the data to ensure timeliness and coverage. Crowdsourced mapping platforms, such as Mapillary<sup>3</sup> and Kartaview,<sup>4</sup> collect data through user contributions, where individuals use smartphones or other devices to capture and upload SVIs. This crowdsourcing approach supplements the coverage of commercial services and improves the diversity and timeliness of the data. Processing SVI generally involves the use of computer vision models to compute various environmental indices, such as SVF (Liang et al., 2017), GVI (Yu, Her, Huo, Chen, & Qi, 2022), and BVI (Gong et al., 2018). These indices can be calculated using different methods, including edge detection (Zeng et al., 2018), and semantic segmentation. Semantic segmentation employs deep learning models (e.g., DeepLab) to perform pixel-level classification of elements within SVI (Xia, Yabuki, & Fukuda, 2021b; Yi et al., 2025; Zhao, Liang, Tu, Huang, & Biljecki, 2023). This process identifies and quantifies the proportions of vegetation, sky, buildings, and other elements in the images.

SVI finds extensive applications in urban research, such as greening assessment, street vitality analysis, urban transportation, and sanitation research (Chen, Zhou, & Li, 2020; Li, Yabuki, & Fukuda, 2022; Liang, Chang, Gao, Zhao, & Biljecki, 2024; Wang, Sun, Yi, Grekousis, & Dong, 2025; Wu, Ye, Gao, & Ye, 2023; Yi et al., 2024). For example, Xia, Yabuki, and Fukuda (2021a) proposed a method that uses semantic segmentation of SVIs to calculate the panoramic view GVI for assessing urban greenery. This scalable and automatable method offers accurate vegetation detection, enhancing urban planning efforts. In a study by Ma (2023), a comprehensive framework was developed combining street scene images, POI data, and deep learning algorithms to analyze urban vitality in Qingdao City. The findings reveal that visual perception factors significantly influence urban vitality, emphasizing the need for street beautification and humanized design in urban planning. However, current research has limitations in handling the uncertainties associated with SVI, particularly those arising from seasonal bias (Chen & Biljecki, 2023; Han et al., 2023). These bias can cause significant differences in

images of the same location taken in different seasons, which can affect the accuracy of environmental indices calculated from these images. Addressing these uncertainties is crucial for improving the reliability of SVI in urban environmental assessments.

## 2.2. Seasonal changes and variability of SVI

Research on SVI time series analysis has garnered increasing attention in recent years, as SVI collection can occur at different times, providing temporal snapshots of urban environments (Hou et al., 2024). Variability in data collection times introduces a new analytical dimension, allowing researchers to track and analyze temporal changes in urban landscapes. For example, time series analysis of SVI can be used to monitor the growth of urban vegetation (Li, 2021; Yu et al., 2022), changes in urban landscapes (Koji et al., 2023; Wang, Ito, & Biljecki, 2024), and the evolution of commercial activities (Li & Long, 2019). In a study by Han et al. (2023), multitemporal SVI was used to characterize seasonal bias in street greenery in Nanjing, China. The findings identified four distinct greening patterns and highlighted the importance of seasonal monitoring for sustainable urban greening design and planning. Liang, Zhao, and Biljecki (2023) proposed an embedding-driven clustering approach to analyze the spatio-temporal evolution of Singapore's visual environment. The research identified six visual clusters from street view imagery, revealing trends such as the growth of high-density visual experiences in new towns and an increase in visually pleasant areas, demonstrating a novel method for urban planning and landscape improvement.

On the one hand, the temporal characteristics of SVI offer new opportunities for observing urban changes. On the other hand, ignoring the collection time of SVI and controlling for seasonality can significantly impact the analysis results. Seasonal bias leads to substantial differences in vegetation cover (Zhang et al., 2022), lighting conditions, and street activity levels in SVIs, affecting the accuracy of environmental indices such as the GVI. For example, winter images may underestimate greenery due to reduced vegetation, while summer images may overestimate it (Qi et al., 2024). In addition, seasonal changes can alter visible street features, leading to misinterpretation of urban landscape

<sup>3</sup> <https://www.mapillary.com/>

<sup>4</sup> <https://kartaview.org/map/>

characteristics (Shukla & Jain, 2019). Therefore, considering seasonal bias is essential to improve the reliability and validity of urban environmental assessments.

The seasonal bias in SVI data refers to the variability in analysis results caused by various parameters. These parameters include the source of the data, the time of data collection, and the methods of spatial sampling. Biljecki et al. (2023) proposed an analytical framework to examine differences in analysis results due to varying data sources, including panoramic and perspective images. The study investigated various methods for estimating indicators such as SVF and GVI using both panoramic and perspective SVIs. The results indicate that street view photos from consumer cameras at single angles often produce results comparable to those from commercial panoramic images. This work demonstrates the value of integrating diverse image sources for urban environmental analysis, especially in the era of crowdsourcing geographic information (Yan et al., 2020). In a study by Kim et al. (2021), the sensitivity of Google Street View (GSV) for streetscape measurements in Santa Ana, California, was empirically assessed. The findings revealed that the measurement results vary significantly with changes in the GSV acquisition parameters, such as spacing and direction, especially for targets such as humans, objects, and sidewalks. This highlights the need to carefully consider GSV settings in urban analysis to ensure accurate results.

### 3. Problem statement

The presence of seasonal bias in SVI is influenced by a combination of climatic, geographic, and urban morphological factors, as well as by the nature of data acquisition itself. This section introduces a conceptual model that links these components, clarifying how each contributes to or mitigates the manifestation of seasonal bias. This part lays the theoretical foundation for the methodological steps described in the following sections.

#### 3.1. Definition 1: seasonal bias in SVI

Seasonal bias in SVI is defined as the systematic discrepancy in indicators of urban form, such as GVI, BVI, or SVF which arises solely due to the timing of data capture rather than actual changes in the built environment. Formally, let  $X_{s,i}$  represent the measured value of an indicator  $X$  (e.g., GVI) for location  $i$  during season  $s$  (spring, summer, autumn and winter). Seasonal bias occurs when

$$X_{s_1,i} - X_{s_2,i} \neq 0 \quad (1)$$

solely as a result of natural seasonal phenomena (e.g., vegetation leaf-on vs. leaf-off), independent of any morphological transformation.

#### 3.2. Definition 2: urban form indicators

Urban form indicators are metrics derived from street-level images to describe specific elements of the urban environment. These three indices, GVI, BVI, and SVF are fundamental urban morphological measures that reflect the distinct dimensions of the streetscape. While GVI is most sensitive to phenological changes, it can also indirectly alter the other two by obscuring or exposing buildings and sky areas. Accordingly, BVI and SVF are included to provide a more holistic understanding of how seasonal biases may propagate through multiple elements of urban form.

#### 3.3. Definition 3: climatic and geographic drivers

Climatic and geographic drivers refer to environmental factors, primarily latitude, temperature, precipitation, and vegetation phenology, that shape how seasons manifest in different cities. In higher-latitude areas, pronounced winters and leaf-off conditions can strongly alter

street-level imagery, while tropical or subtropical climates have more uniform greenery year round. In regions with stark climate changes (e.g., monsoonal rainfall or large temperature swings), the contrast between leaf-on and leaf-off seasons is amplified, making seasonal bias in SVI more evident.

### 4. Methodology

The proposed methodological framework, as illustrated in Fig. 2, is divided into two main stages: (1) data collection and pre-processing and (2) seasonal bias analysis. The first stage consists of three core steps. First, 40 cities around the world were selected as study areas based on criteria such as geographical diversity, climate diversity, and the richness of SVI. Because this phenomenon varies around the world and will likely affect SVI-powered studies in different ways, it is imperative to include dozens of cities distributed globally. Then, several sampling points were chosen within each city, with SVIs captured for each sampling point in spring, summer, autumn, and winter. Finally, a semantic segmentation model was used to calculate urban form indicators for each sampling point in each season.

In the second stage, seasonal bias analysis was conducted from three perspectives. From the perspective of individual cities, three metrics such as MAE, MAPE, and R were used to evaluate seasonal bias in SVIs and analyze their spatial distribution patterns. From the global perspective, a standardized index  $B_X$  was used to quantify the seasonal bias for each city, explain these biases with urban climate factors (e.g., precipitation and temperature) and explore their spatial distribution patterns. From the perspective of practical applications of SVI, different combinations of seasonal data were simulated to perform urban function classification, analyzing the impact of seasonal bias in practical applications, and understanding the degree of bias.

#### 4.1. Data collection and preprocessing

##### 4.1.1. Collection of SVI

In this study, Google Street View (GSV) image was used as a data source. This commercial source provides high spatial coverage, a sufficient sampling frequency, and high-quality images, ensuring the collection of data for all four seasons at a sampling location. Furthermore, focusing on a single data source minimizes the possible bias of using different acquisition approaches (e.g., two different providers may use different panoramic cameras and acquisition practices). The GSV data were downloaded using the open source tool streetview.<sup>5</sup> With this tool, multiple panoramic SVIs can be obtained around a sampling location by entering the latitude and longitude coordinates of the location. These SVIs may be collected in different years and seasons. Google API<sup>6</sup> was utilized to acquire metadata for the SVIs, such as timestamps, which were used to determine the season in which the images were captured. To ensure consistency in the perspectives of all collected images, these panoramic images were processed to various viewing angles (Biljecki et al., 2023). The camera was configured to face directly forward with a field of view (FOV) set to 120 degrees.

To ensure that the observed changes in SVI indicators primarily reflect seasonal bias, rather than being influenced by urban renewal or other external factors, it is necessary to carefully filter the raw collected data. The detailed steps of this filtering method are as follows:

- *Spatial range control:* The primary objective is to select a SVI at a sampling location for each of the four seasons, ensuring that they are sufficiently similar to exclude errors caused by scene changes due to spatial mismatch. The specific approach involves selecting SVI data from four different seasons within a defined spatial range for comparison. We

<sup>5</sup> <https://github.com/robolyst/streetview>

<sup>6</sup> <https://developers.google.com/maps/documentation/streetview>

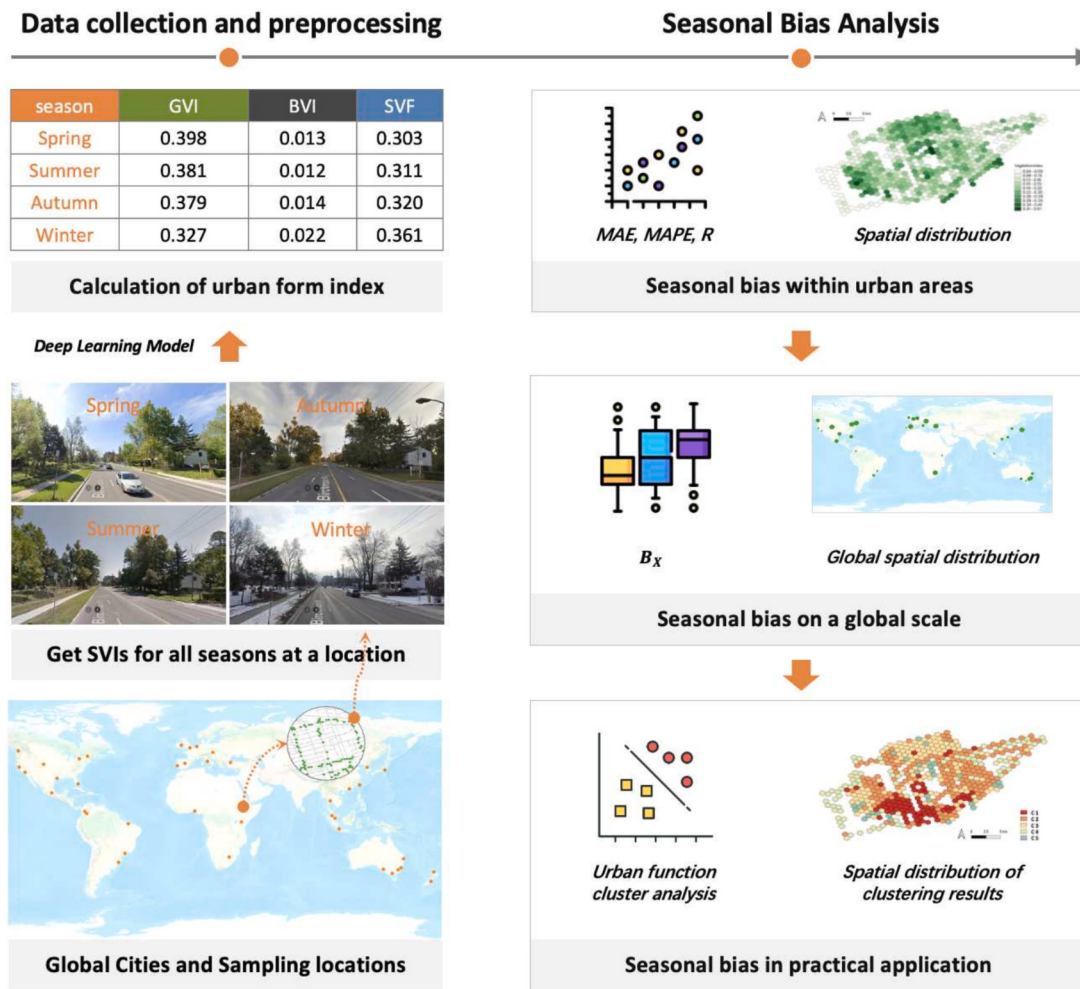


Fig. 2. A framework for analyzing seasonal bias in SVI.

employ the H3 spatial indexing system<sup>7</sup> to generate hexagonal level 12 grids, each covering an area of approximately 307.092 m<sup>2</sup>. At H3 index level 12, the maximum distance between any two points within a single hexagon does not exceed 18.83 m, ensuring a sufficiently localized spatial scope for subsequent analyzes.

- **Temporal interval control:** To minimize the effects of urban renewal, the study selects data collected during the same or closely related years. Within each spatial grouping, the data is further filtered by year to ensure that all images used for comparison fall within a similar temporal window, specifically within a 5-year range.

It should be noted that, in some areas, SVI data collection is not frequent enough, which may result in the absence of suitable data for certain spatial units. These areas will be excluded from the consideration. This study categorizes the SVI into different seasons based on the metadata's capture date. Given the seasonal inversion between these hemispheres, the definition of seasons is adjusted accordingly: for cities in the Northern Hemisphere, December to February is considered winter, March to May as spring, June to August as summer, and September to November as autumn. Conversely, for cities in the Southern Hemisphere, the seasonality is reversed, with June to August designated as winter, and so forth.

#### 4.1.2. Calculation of urban form index

Although the bias in vegetation coverage makes the GVI particularly

sensitive to seasonal changes, the BVI and the SVF can also exhibit a notable seasonal bias. In winter, for example, withered trees can expose more building facades, thereby increasing the BVI and decreasing the GVI. In contrast, when vegetation is dense in summer, parts of the sky or building surfaces could be obscured by leaves, thereby reducing SVF or BVI while increasing GVI. Hence, seasonal bias in our work is not exclusively limited to the GVI; we systematically evaluate its impact on all three indices to obtain a more comprehensive understanding of how seasonal factors could skew SVI-based urban assessments. These indices represent the proportion of the corresponding elements within the entire image. They are widely used in urban landscape planning, land use analysis, and other related fields (Cao et al., 2023; Ito & Biljecki, 2021; Xia et al., 2021a).

Semantic segmentation is a common deep learning technique used to calculate these indices. This technique performs pixel-level classification on images, allowing for the accurate identification and segmentation of different elements within the image, such as vegetation, sky, and buildings. Among the numerous models developed for semantic segmentation, EfficientViT stands out as an innovative high-resolution vision model, distinguished by its novel multiscale linear attention mechanism (Cai, Li, Hu, Gan, & Han, 2023). The training data set used in this study is Cityscapes, a large-scale data set renowned for its comprehensive collection of SVIs from various urban settings in cities.<sup>8</sup> Cityscapes is meticulously annotated, providing detailed pixel-level

<sup>7</sup> <https://h3geo.org/docs/core-library/restable>

<sup>8</sup> <https://www.cityscapes-dataset.com/>

annotations for a wide range of categories, including but not limited to roads, vehicles, buildings, vegetation, and sky. The EfficientViT model, trained on the Cityscapes dataset, demonstrated a mean Intersection over Union (mIoU) accuracy of 83.228. This precision can ensure the correctness of the calculation of the GVI, SVF, and BVI.

#### 4.2. Seasonal bias assessment framework

Seasonal bias refers to the differences in measuring urban form indicators or analysis results caused by natural and environmental changes between different seasons. It is important to note that no single season's calculated indicators can be considered "correct" or "standard." Rather, seasonal bias serves to quantify the variations between seasons, without implying that one season's results are more accurate than another. In the previous step, semantic segmentation techniques were used to extract three key urban form indicators, BVI, SVF, and GVI from each SVI. The distribution of these indicators in each season can be obtained based on the collection time and location of the SVIs. This study analyzes seasonal bias in SVI from three perspectives: within urban areas, on a global scale, and in practical applications.

##### 4.2.1. Intra-urban seasonal bias assessment

In order to assess the seasonal bias within a city across different seasons, we employ three complementary metrics: Mean Absolute Error (MAE), Mean Absolute Percentage Error (MAPE), and Pearson's correlation coefficient ( $R$ ). For each location  $i$ , let  $X_{s_1,i}$  and  $X_{s_2,i}$  represent the measured values of an urban form indicator  $X$  (e.g., BVI, SVF, GVI) in two distinct seasons  $s_1$  and  $s_2$ . With  $n$  denoting the total number of locations sampled and  $\bar{X}_{s_1}$  and  $\bar{X}_{s_2}$  as mean values of  $X$  in these two seasons, the metrics are defined as follows:

$$MAE = \frac{1}{n} \sum_{i=1}^n |X_{s_1,i} - X_{s_2,i}|, \quad (2)$$

$$MAPE = \frac{1}{n} \sum_{i=1}^n \left| \frac{X_{s_1,i} - X_{s_2,i}}{\bar{X}_{s_1}} \right| \times 100\%, \quad (3)$$

$$R = \frac{\sum_{i=1}^n (X_{s_1,i} - \bar{X}_{s_1})(X_{s_2,i} - \bar{X}_{s_2})}{\sqrt{\sum_{i=1}^n (X_{s_1,i} - \bar{X}_{s_1})^2} \sqrt{\sum_{i=1}^n (X_{s_2,i} - \bar{X}_{s_2})^2}}. \quad (4)$$

By comparing these three statistics, we can capture the absolute discrepancy (MAE), the relative discrepancy (MAPE), and the rank-based consistency ( $R$ ) in seasonal measurements of urban form indicators, thus quantifying the extent of seasonal bias. These three metrics offer a comprehensive approach to assessing seasonal deviations from multiple perspectives.

- MAE: Measures the absolute deviation within a single city, reflecting how indicators differ between seasons (e.g., summer vs. winter). Although MAE may be misleading in cross-city comparisons (owing to different baselines), it remains valuable for quantifying the scale of seasonal change within an urban area.

- MAPE: Captures relative deviations, thus facilitating more equitable cross-regional or cross-city comparisons. By normalizing the values, MAPE addresses the disparities in the levels of the baseline indicator. However, caution is needed if an indicator approaches zero, as this may yield disproportionately large percentages.

- Pearson's R: Although absolute and relative errors gauge the degree of numerical deviation, it is also crucial to assess how consistently the indicator values of an area rank over seasons. Pearson's R measures whether locations with high (or low) values in one season remain correspondingly high (or low) in another, thus capturing the spatial coherence of seasonal changes.

To further explore the spatial distribution patterns of seasonal bias, the three urban form and seasonal bias indicators were aggregated into predefined spatial units. Specifically, the H3 geospatial indexing system

was utilized, setting the size of each spatial unit at H3 level 8, with an area of approximately  $0.737 \text{ km}^2$ .

##### 4.2.2. Global-scale seasonal bias quantification

Before performing a global scale analysis, it is necessary to define an indicator to evaluate seasonal bias on the city scale. We adopt the following two-step procedure: The first step is to quantify the seasonal bias at the point level. Let  $X_{s,i}$  be the value of a chosen indicator  $X$  (e.g., GVI, BVI, or SVF) at location  $i$  in season  $s$ , where  $s$  can be spring, summer, autumn, or winter. The seasonal bias at the point level is the standard deviation for each sampling location  $i$ :

$$\sigma_i = \text{std}(X_{\text{spring},i}, X_{\text{summer},i}, X_{\text{autumn},i}, X_{\text{winter},i}) \quad (5)$$

Then, aggregating bias at the city scale. Suppose that the city has  $N$  valid sampling locations. We aggregate the standard deviations per point  $\sigma_i$  taking their average:

$$B_X = \frac{1}{N} \sum_{i=1}^N \sigma_i \quad (6)$$

Here,  $B_X$  represents the city-level seasonal bias for the chosen indicator  $X$ , capturing the overall magnitude of bias when transitioning among spring, summer, autumn, and winter. A larger  $B_X$  implies the city experiences more pronounced seasonal changes in  $X$ , whereas a smaller value indicates relative stability across seasons.

To quantitatively assess how climatic characteristics affect  $B_X$ , we incorporate an OLS regression. In this approach, the  $B_X$  served as the dependent variable, while four predictors, namely the standard deviations and mean values of rainfall and temperature, were chosen to capture both the magnitude and variability of local weather conditions. We source these climate indicators from worldclim,<sup>9</sup> ensuring temporal alignment with our SVI sampling periods. In addition, to investigate the pattern of seasonal bias, we performed a cluster analysis. For each of the 40 cities, we used five climate and geographic characteristics as inputs: mean and standard deviation of temperature, mean and standard deviation of rainfall, and absolute latitude. After normalizing these features, we applied the k-means algorithm, determining via the elbow method.

##### 4.2.3. Evaluating seasonal bias impact on practical applications

To evaluate the impact of seasonal data bias on practical applications, this study investigates the errors introduced by different combinations of seasonal data through a case study of urban functional analysis. Urban functional analysis using SVI is a common application in street view research. As illustrated in Fig. 3, by extracting the vegetation, building, and sky features from SVIs and analyzing their proportions, the urban morphological types can be inferred. For instance, areas dominated by buildings are likely to be central business districts; areas dominated by vegetation may be natural scenic areas; and areas where the sky is predominant, along with some vegetation coverage, are likely to be suburban regions. Referencing literature by Liang et al. (2023), these three characteristics of a graph are input into an unsupervised clustering algorithm of k-means to categorize the city into different functional zones.

This study constructs four validation scenarios using different seasonal data combinations to assess the impact of data sampling on urban functional analysis. These scenarios are defined as follows:

- Latest data: Using 10,000 of the most recently captured SVIs.
- Random sampling: Randomly sampling SVIs taken over the past five years.
- Summer data: All data is sourced from images taken during the summer.
- Winter data: All data is sourced from images taken during the winter.

<sup>9</sup> <https://www.worldclim.org/data/index.html>

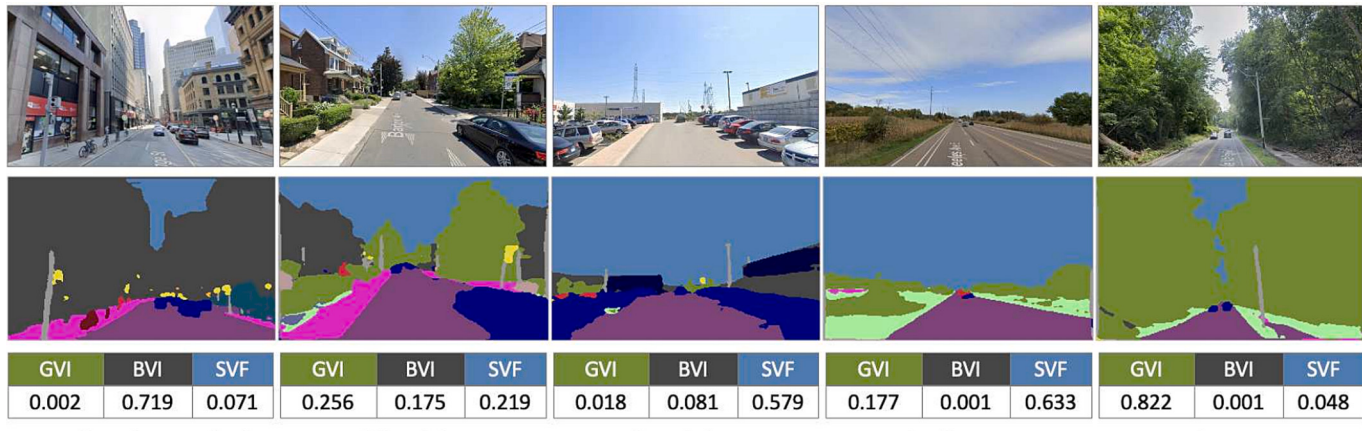


Fig. 3. SVI data analysis of different urban functional areas.

Spatial units are delineated using hexagonal H3 grids with a resolution of level 8,<sup>10</sup> calculating the average values of vegetation, building, and sky characteristics for each spatial unit. These features are used as input to the k-means unsupervised clustering algorithm to classify the city into functional zones. In this study, the value of  $k$  is set to 5, categorizing the city into five distinct functional zones.

To quantitatively assess differences in the clustering results, this study uses the Adjusted Rand Index (ARI) to compare the clustering results of Vienna and Toronto under the four different data scenarios (Santos & Embrechts, 2009). ARI measures the similarity or consistency between two clustering results, with a value of 1 indicating complete agreement and 0 indicating random alignment. Formally, let  $X$  and  $Y$  be two clustering solutions on  $N$  samples, and denote by:  $a =$  the number of pairs of samples assigned to the same cluster in both  $X$  and  $Y$ ,  $b =$  the number of pairs of samples assigned to different clusters in both  $X$  and  $Y$ . The Rand Index (RI) is then defined as:

$$RI = \frac{a + b}{\binom{N}{2}} \quad (7)$$

where  $\binom{N}{2}$  is the total number of distinct pairs among the samples  $N$ .

The ARI further incorporates an adjustment for chance as follows.

$$ARI = \frac{RI - E[RI]}{max(RI) - E[RI]} \quad (8)$$

where  $E[RI]$  is the expected value of the Rand index under a hypergeometric distribution assumption, and  $max(RI)$  is the maximum value the Rand Index can take. In this study, rather than comparing our clustering results to an external “ground truth,” we used ARI to assess how consistent the identified clusters remain when the underlying streetview data are sampled in different seasons. A higher ARI indicates that two clustering configurations, for example “summer data” vs. “winter data,” assign samples (e.g., spatial units) more similarly, thus reflecting lower seasonal bias.

## 5. Experiment and results

### 5.1. Dataset summary

In this study, SVIs were collected from 40 cities in 25 countries. These cities were selected to ensure the sufficient quantity of Google

Street View data in the dataset, climate diversity, geographic diversity, and variety on the urban scale. The details of the dataset are listed in Table A.1. Using the methods described in Section 4.1, image data was collected from 65,747 locations. For each location, SVI were obtained for the four seasons, spring, summer, autumn, and winter totaling 262,988 images. Semantic segmentation models were used to extract three indicators from each image: buildings, vegetation, and sky, which were then utilized for subsequent analysis.

### 5.2. Analysis of intra-urban seasonal bias in SVI

#### 5.2.1. An intuitive understanding of seasonal bias

The seasonal bias in SVI is illustrated through an intuitive comparison between two climatically distinct cities: Singapore and Toronto. Due to Singapore’s equatorial climate, characterized by consistently high humidity and abundant rainfall throughout the year, the city has no distinct true seasons and experiences almost no seasonal bias throughout the year. Toronto experiences a temperate continental humid climate characterized by warm, humid summers and cold winters, with clear seasonal distinctions and evenly distributed precipitation.

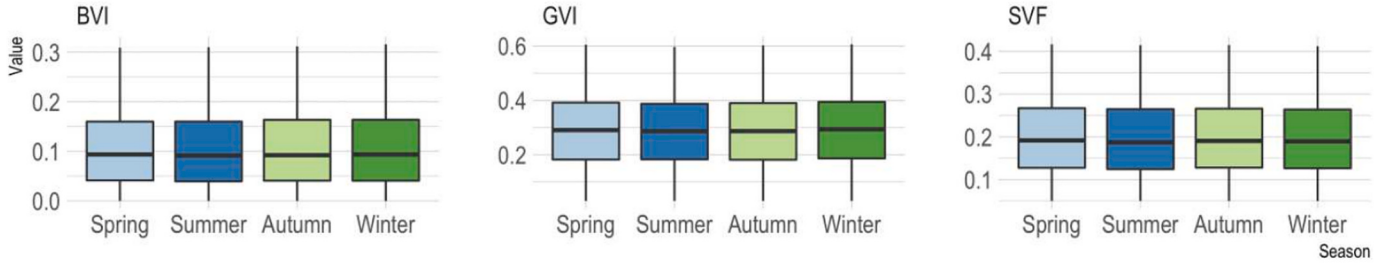
Box plots were used to represent the bias in three indicators of urban form in different seasons, as shown in Fig. 4. Overall, the three indicators for Toronto exhibit significant fluctuations throughout the four seasons, whereas those for Singapore remain relatively stable. Taking the GVI as an example, Singapore shows minimal bias in all four seasons, with a median between 0.288 and 0.294. However, in Toronto, the median falls between 0.150 and 0.179. In cities with different seasons, it is evident that seasonal changes significantly affect the GVI. During winter, the GVI decreases due to leaf fall, as there is less vegetation cover. At the same time, the BVI increases due to reduced tree obstruction. For instance, in Toronto, the GVI drops from 0.179 in summer to 0.150 in winter, while the BVI rises from 0.045 to 0.066.

Given the pronounced seasonal bias in Toronto, this city is used as an example to visually analyze the seasonal bias in SVI through specific scenarios. As shown in Fig. 5, the color of the spatial hexagons represents the magnitude of the MEA between the GVI in summer and winter for the area. A comparative analysis is conducted by selecting two original images from summer and winter, along with their corresponding semantic segmentation results.

- The scene ① is a park. In summer, dense foliage results in high GVI. Despite the loss of leaves in winter, the tree outlines remain distinct, allowing the semantic segmentation algorithm to recognize most of the vegetation, resulting in a small bias in the GVI between the two seasons.

<sup>10</sup> <https://h3geo.org/docs/core-library/restable>

## Singapore



## Toronto

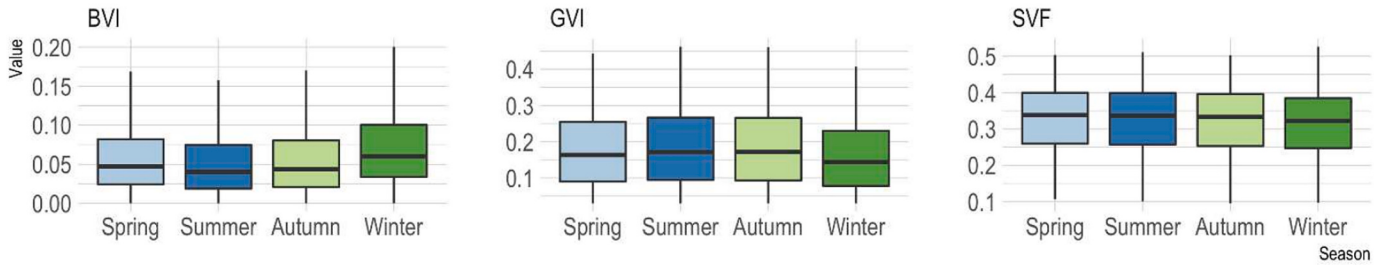
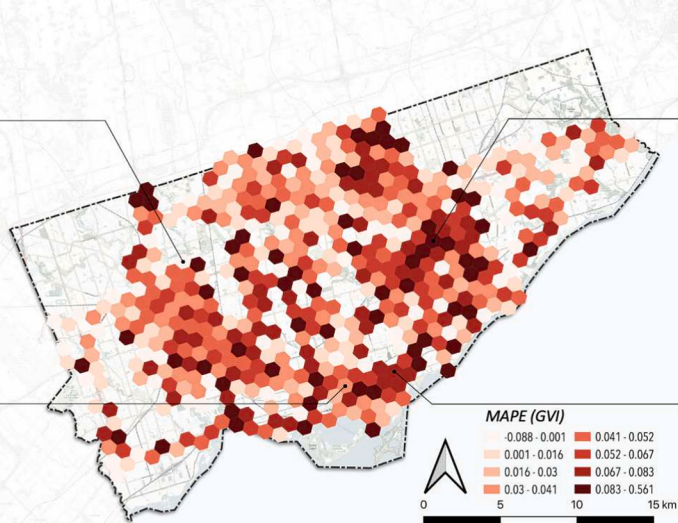
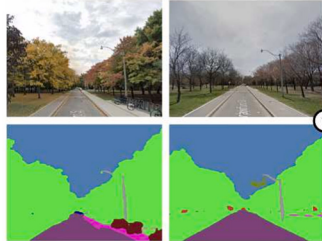
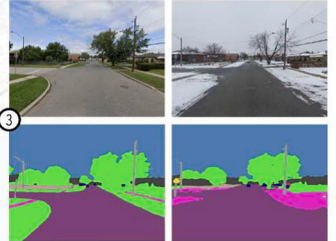


**Fig. 4.** Bias in urban form indicators in different seasons.

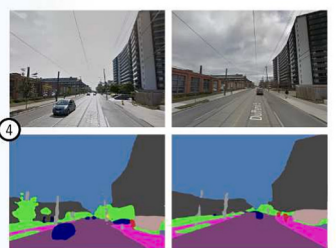
### Small bias (MAPE)



### Medium bias (MAPE)



### Large bias (MAPE)



### Medium bias (MAPE)

**Fig. 5.** An intuitive understanding of seasonal bias using GVI as an example (Toronto).

- The scene ② is a commercial district in the city center. In summer, a small amount of vegetation can be identified, such as trees and plants. However, in winter, with the vegetation withered, there is almost no recognizable vegetation, leading to a large bias in the GVI between the seasons. This suggests that in high-density urban environments, such as commercial districts, the GVI is highly influenced by seasonal changes.
- The scene ③ is a suburban area, where the GVI is high in the summer due to extensive grass and tree cover. However, in winter, the grass is covered with snow, resulting in a significant reduction in the GVI and creating a substantial seasonal bias.

- The scene ④ is a residential area, where the distinction between trees and buildings becomes difficult in winter. The MAE of the GVI between winter and summer is distinct. This scenario highlights that in areas with mixed vegetation and buildings, seasonal changes can significantly affect the accuracy of the GVI calculations.

#### 5.2.2. Quantitative assessment of seasonal bias

Quantitative assessment of seasonal bias was performed using three indicators: MAE, MAPE, and R. As shown in Table A.2, the mean MAE for the three indicators, GVI, BVI, and SVF in global cities are 0.071, 0.046, and 0.052, respectively. These results suggest that, on average,

the GVI exhibits the largest seasonal deviation among the three metrics, likely reflecting the higher sensitivity of vegetation to seasonal changes. In contrast, although the MAE values for BVI and SVF are relatively small, they remain noteworthy. They still undergo changes due to bias in vegetative cover or weather conditions (e.g., snowfall). Taking GVI as an example, the highest MAE occurs in Singapore. From the previous analysis, it can be inferred that although Singapore exhibits minimal seasonal bias. However, the high vegetation coverage, which results in a higher GVI value, contributes to the larger MAE for GVI. Therefore, using MAE to measure seasonal bias might be somewhat misleading.

From the perspective of MAPE, the average MAPE values for GVI, BVI and SVF are 54.203 %, 857.216 %, and 22.238 %, respectively (Table A.2). For GVI, the cities with the highest and lowest MAPE are Montreal and Singapore, respectively, which aligns with the analysis in Section 5.2.1. Fig. 6 illustrates the distribution of MAPE in two representative cities, Vienna and Toronto, stratified into three groups according to their GVI levels: high, medium, and low. In particular, areas with higher GVI (high group) exhibit significantly smaller seasonal bias in MAPE. In Vienna, the median MAPE in the high group is only 1.44 %, compared to 12.96 % in the low group. A similar trend is observed in Toronto, where the median MAPE increases from 9.84 % in the high group to 25.36 % in the low group. The high group often corresponds to large urban parks or areas with dense tree canopy, where vegetation remains visible even in winter, leading to smaller seasonal differences. In contrast, the low group typically includes areas with sparse or scattered greenery that are more susceptible to seasonal loss. Furthermore, since MAPE is influenced by the baseline GVI value in winter, a lower winter GVI can result in inflated relative differences, even when the absolute change is minor. Together, these factors contribute to the larger apparent seasonal bias observed in the low-GVI group.

Spatial visualizations of GVI groupings and MAPE were performed to explore the spatial distribution patterns of vegetation bias. As shown in Fig. 7, the upper half of the figure illustrates the distribution of GVI in different spatial units (H3 units) in each city, classified into high, medium and low groups. The lower half of the figure displays the corresponding spatial distribution of seasonal bias in the GVI. In Vienna, areas with higher GVI are mainly located in the southeast and northwest regions, which probably include parks and nature reserves with extensive greenery. The MAPE shows significant bias across different regions but exhibits a certain degree of spatial clustering, with a global Moran's I value of 0.312 (Anselin, Bera, Florax, & Yoon, 1996). In Toronto, the GVI distribution also reveals noticeable spatial differences, with higher GVI areas concentrated around the city's periphery. Areas with higher seasonal vegetation bias are mainly located in the central-eastern part of the city and also show clear spatial clustering, with a Moran's I value of 0.456.

From the perspective of R, in the 40 global cities, the mean R between summer and winter is highest for SVF (mean  $R = 0.772$ ), followed

by BVI (mean  $R = 0.712$ ) and lowest for GVI (mean  $R = 0.674$ ), indicating stronger seasonal variability in vegetation, as shown in Table A.2. In particular, tropical cities such as Singapore and Taipei show very high R values for GVI (0.938 and 0.934, respectively), while temperate cities such as Istanbul and Los Angeles exhibit much lower GVI correlations (0.316 and 0.059), reflecting substantial seasonal fluctuation. Taking Vienna and Toronto as examples, the correlation between different urban form indicators across seasons is analyzed, as shown in Table 1. High correlation coefficients indicate strong consistency of these indices between seasons, demonstrating stability in certain indices despite seasonal changes. In general, both cities show high correlations in BVI and SVF throughout the seasons, suggesting that these structural elements are less affected by seasonal bias. However, the GVI in both cities shows a more pronounced seasonal bias, with significant differences observed in the indices during contrasting seasons. Specifically, in Vienna, the SVF achieves the highest correlation, reaching 0.943, indicating minimal seasonal bias in sky view. The correlation for GVI is relatively lower, with a maximum value of 0.87. A similar pattern is observed in Toronto, where the BVI and the SVF also show high correlations between seasons, with the SVF reaching a maximum of 0.937 between autumn and summer. The GVI shows a lower correlation, especially between summer and winter (0.822), indicating a greater seasonal variability in vegetation.

### 5.3. Global-scale seasonal bias patterns in SVI

Table A.3 presents the seasonal bias results for 40 cities worldwide, where a higher  $B_X$  signifies a stronger seasonal bias in the corresponding urban form indicator X. In all cities sampled, the mean values for  $B_{GVI}$ ,  $B_{BVI}$ , and  $B_{SVF}$  are 0.059, 0.037, and 0.044, respectively. Notably, Istanbul reports the highest  $B_{GVI}$  (0.087), Tokyo exhibits the highest  $B_{BVI}$  (0.065), and Los Angeles records the highest  $B_{SVF}$  (0.063). These findings illustrate how various facets of the urban environment exhibit differential susceptibility to seasonal changes under distinct climatic and geographic conditions. Among these indicators, vegetation bias appear to be the main driver of seasonal fluctuations in street-level imagery. Consequently, the ensuing analysis focuses on  $B_{GVI}$  for a more detailed examination and comparison of global seasonal bias.

This section focuses on GVI as a representative indicator for analyzing global patterns of seasonal bias, as it exhibits clearer seasonal variability compared to other indicators of urban form, such as SVF or BVI, making it more suitable for illustrating climatic and geographic influences. Fig. 8 illustrates the global distribution of seasonal bias in the GVI, denoted as  $B_{GVI}$ , in 40 representative cities around the world. The results reveal notable geographic disparities in the seasonal dynamics of green visibility. Cities located in temperate regions of the Northern Hemisphere, such as Vienna, Rome, London, and Toronto, exhibit relatively high  $B_{GVI}$  values (above 0.069), indicating pronounced

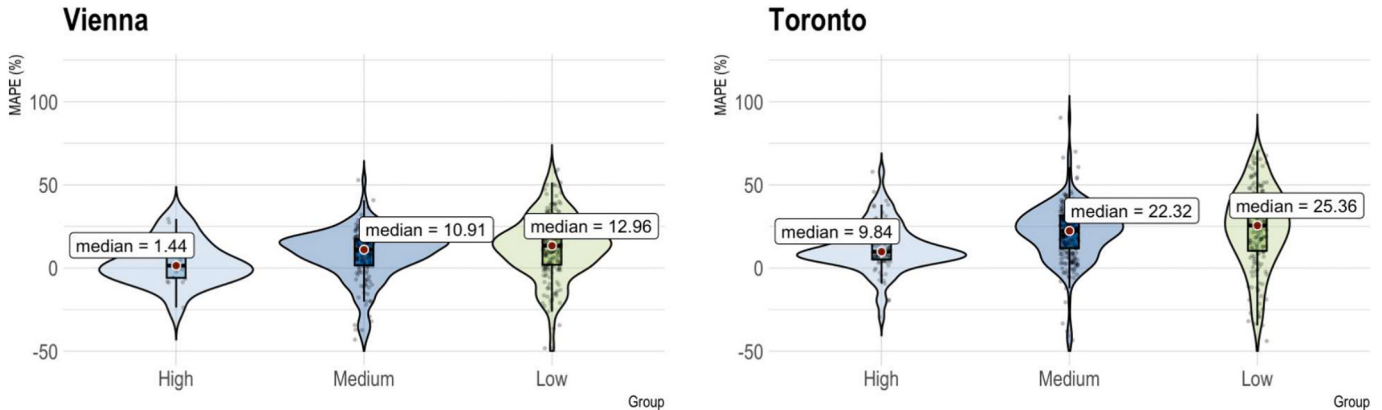
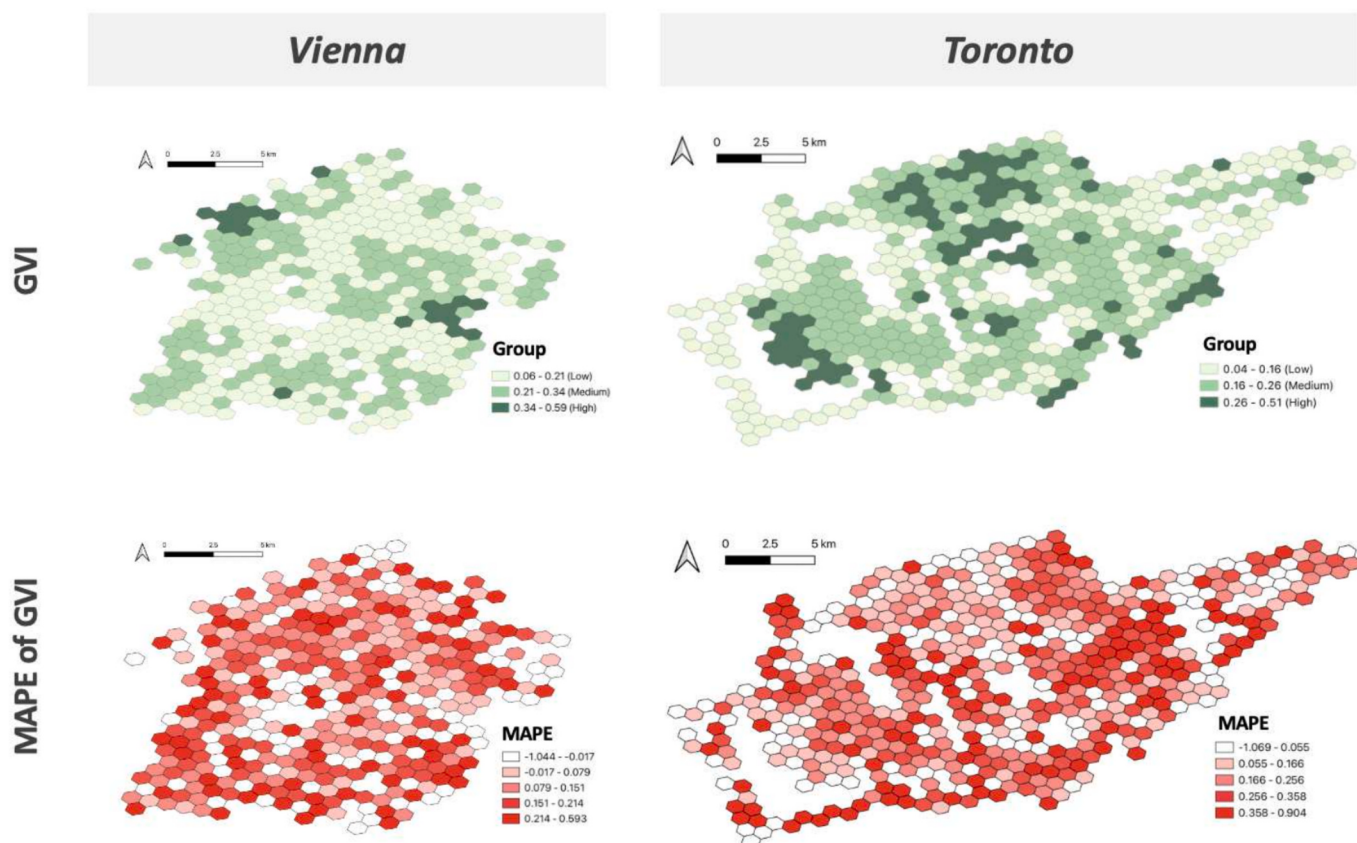


Fig. 6. Seasonal bias of GVI between summer and winter across high, medium, and low GVI areas in Vienna and Toronto, measured by MAPE (%).



**Fig. 7.** Spatial distribution of GVI and its MAPE in summer and winter.

**Table 1**

Pearson correlations between urban form indices in Vienna and Toronto in different seasons.

City	Vienna			Toronto		
	BVI	GVI	SVF	BVI	GVI	SVF
Autumn_Spring	0.910	<b>0.849</b>	0.911	0.878	0.881	0.916
Autumn_Summer	<b>0.873</b>	0.865	<b>0.910</b>	0.861	0.859	0.937
Autumn_Winter	0.922	0.870	0.943	0.882	0.855	0.917
Spring_Summer	0.883	0.855	0.919	0.886	0.851	0.922
Spring_Winter	0.908	0.861	0.928	0.870	0.871	0.919
Summer_Winter	0.888	0.883	0.914	<b>0.857</b>	<b>0.822</b>	<b>0.910</b>

Note: **Bolded** values indicate the minimum Pearson correlation coefficients among the compared seasons, reflecting the largest degree of seasonal bias.

seasonal fluctuations in greenery, likely corresponding to deciduous tree cover and marked transitions between summer and winter vegetation states. Similarly, high deviations are observed in some Australian cities (e.g., Canberra, Adelaide), reflecting comparable seasonal vegetation cycles in the Southern Hemisphere. In contrast, tropical and equatorial cities, including Jakarta, Singapore, Kuala Lumpur, and Bangkok, display low  $B_{GVI}$  values (typically below 0.046), suggesting a more stable year-round green view, consistent with their evergreen vegetation and relatively invariant climatic conditions. African cities such as Nairobi and Lagos, as well as Latin American cities such as Bogota and Sao Luis, also exhibit minimal seasonal bias in the GVI. Interestingly, some North American cities such as San Francisco and Denver demonstrate moderate seasonal deviation, likely due to region-specific climate and urban vegetation patterns. The heterogeneity in the seasonal bias of the GVI between global cities highlights the combined influence of bioclimatic zones, vegetation composition, and urban landscape planning on the dynamics of greenery at the street level.

**Fig. 9** visualizes the spatial bias and climatic associations of seasonal bias in the BVI in 40 global cities. Here, the size of each bubble reflects the values of  $B_{GVI}$  categorized into five equal-interval ranges. The bubble graph maps cities by their mean rainfall (x-axis) and mean temperature (y-axis), with the bubble size proportional to  $B_{GVI}$ . In general, cities in colder and drier regions, such as Montreal, Toronto, and Vienna, exhibit a relatively higher  $B_{GVI}$ , indicating a more pronounced seasonal bias. In contrast, cities in equatorial or tropical regions (for example, Jakarta, Singapore) show lower  $B_{GVI}$ , consistent with evergreen vegetation and limited seasonal changes in canopy cover. This spatial pattern suggests that temperature and precipitation regimes exert a substantial influence on the seasonality of visual greenery in urban environments.

To further explore these relationships, the cities were grouped into three clusters using k-means clustering based on five geographic and climatic variables: mean temperature, temperature standard deviation, mean rainfall, rainfall standard deviation, and absolute latitude. As shown in both **Fig. 9** and the corresponding radar plot in **Fig. 10**, the clusters capture distinct climatic-geographic regimes. Cluster 1 (blue) includes mainly tropical cities with high temperatures, low variability in temperature, and abundant and stable rainfall, conditions that result in consistently low  $B_{GVI}$ . Cluster 2 (red) consists of cities with moderate climates and rainfall bias, leading to intermediate seasonal greenness fluctuation. Cluster 3 (green), on the contrary, represents cities with higher latitudes or continental cities with strong temperature seasonality and higher absolute latitudes. These cities experience pronounced leaf-on/leaf-off transitions, contributing to the highest levels of  $B_{GVI}$ . Together, the results and visualizations of the clustering emphasize that the seasonality of urban greenness is closely intertwined with latitude-driven phenological patterns and local climatic variability.

Building on the spatial pattern analysis presented in the previous figures, we also employed an OLS regression model to examine the extent to which climatic factors contribute to the seasonal deviation of

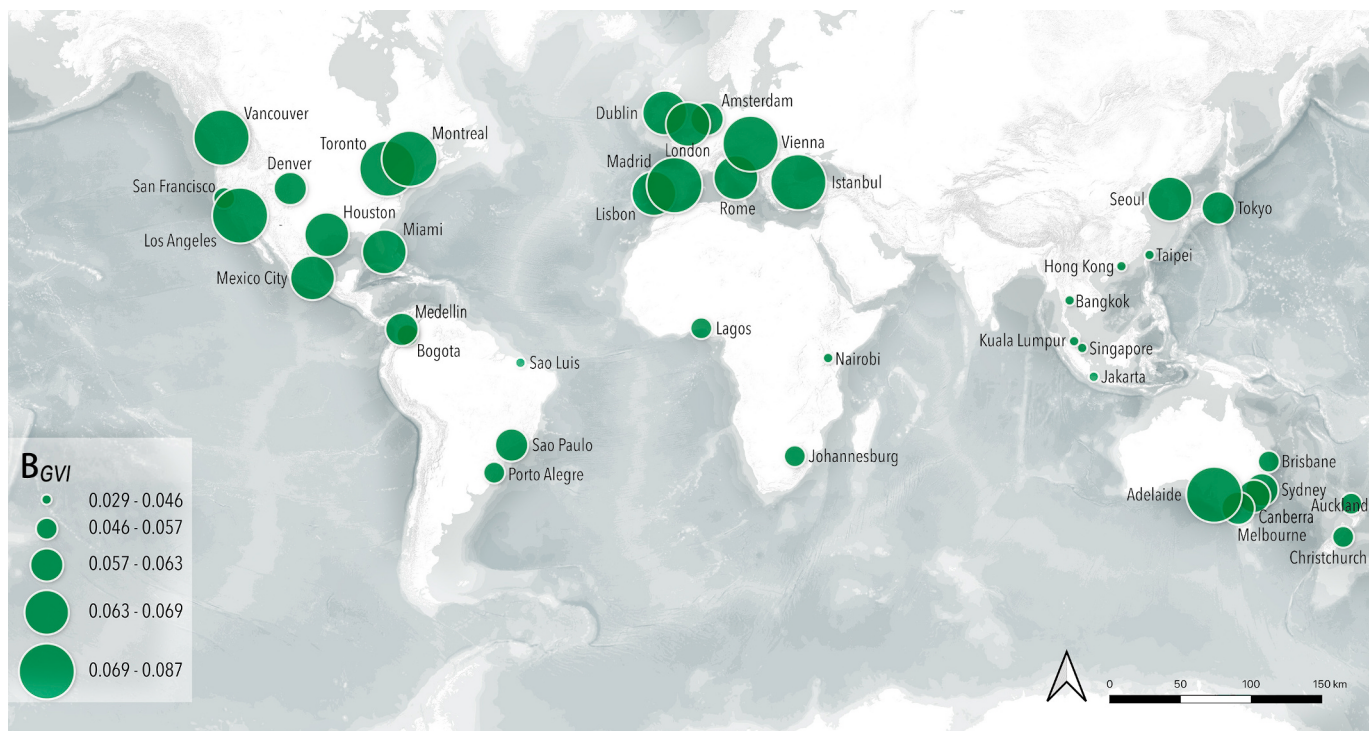


Fig. 8. Global spatial distribution of seasonal bias of GVI Basemap: Esri.

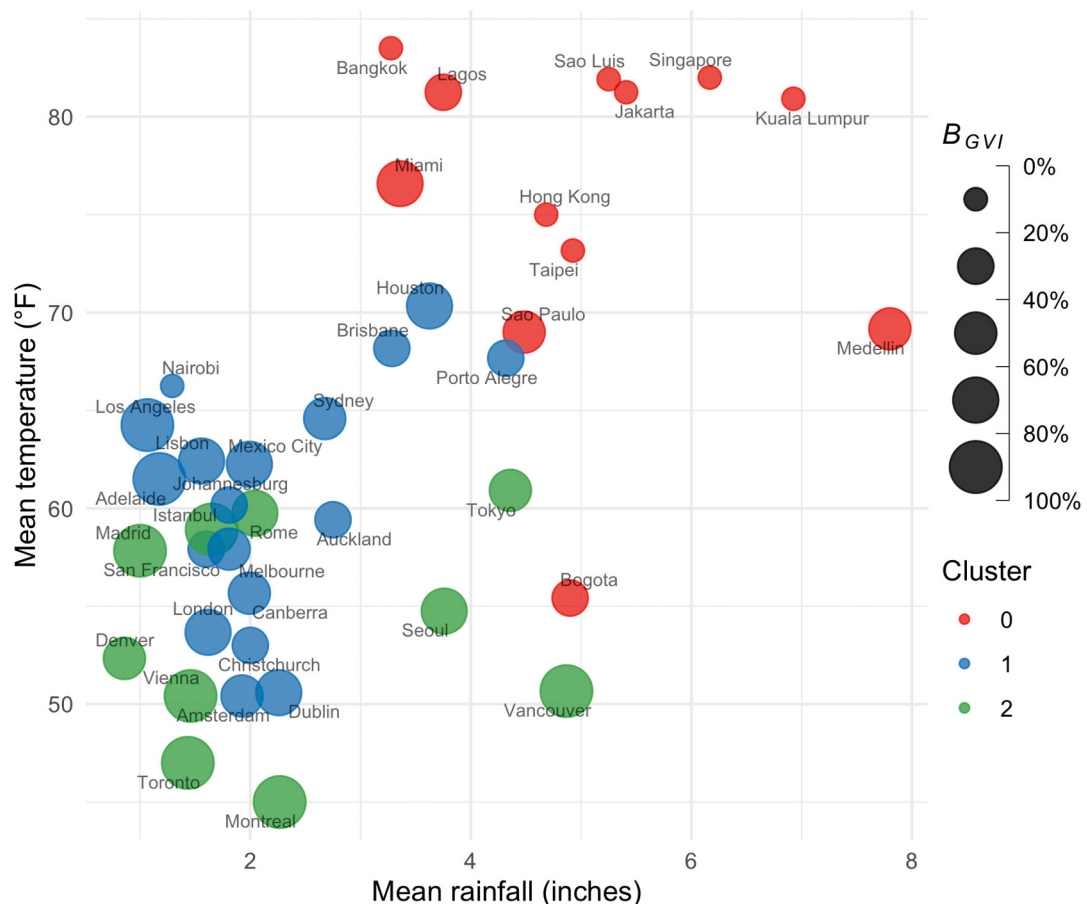
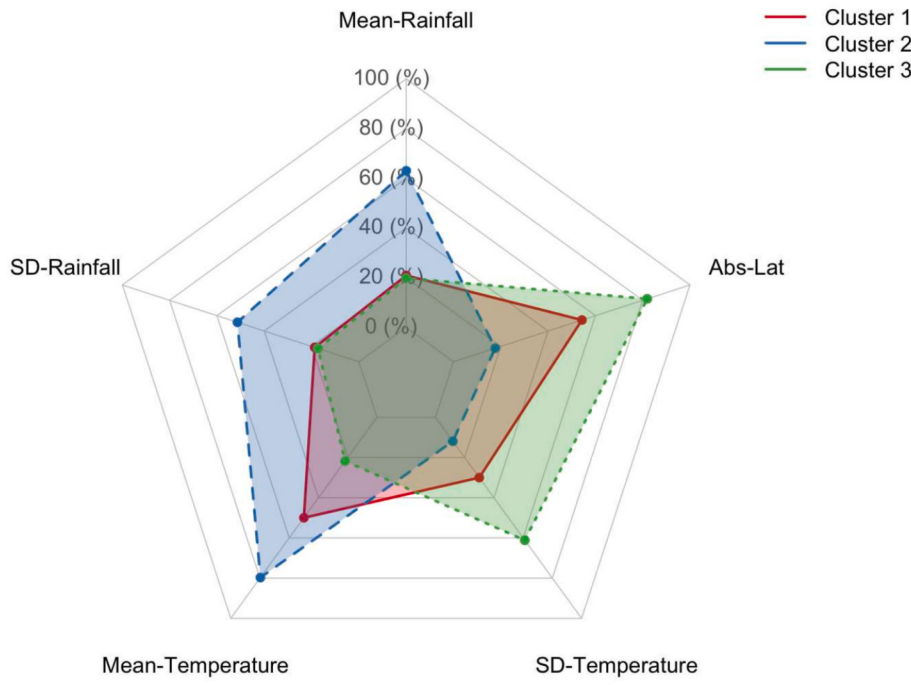


Fig. 9. Visualization of seasonal bias in GVI relative to average temperature and rainfall.



**Fig. 10.** Climatic and geographic metrics for each cluster.

**Table 2**

OLS regression results for the relationship between climatic variables and  $B_{GVI}$ .

Variable	Estimate( $\beta$ )	Std. Error	t value	$Pr( >  t )$	Signif.
(Intercept)	0.0784	0.0165	4.7415	3.49E-05	
SD_Rainfall	-0.0008	0.0020	-0.4366	0.6651	
SD_Temperature	0.0009	0.0004	2.1167	0.0414	*
Mean_Rainfall	-0.0018	0.0013	-1.3506	0.1854	
Mean_Temperature	-0.0003	0.0002	-1.2516	0.2190	

$R^2$ : 0.513, Adjusted  $R^2$ : 0.457, F-statistic: 9.218, p-value: 3.39E-05 Signif. codes: 0 ‘\*\*\*’ 0.001 ‘\*\*’ 0.01 ‘\*’ 0.05.

the vegetation index, denoted  $B_{GVI}$ . The regression results are presented in Table 2. The model demonstrates moderate explanatory power, with an  $R^2$  of 0.513 and an adjusted  $R^2$  of 0.457. The overall model is statistically significant ( $F = 9.218$ ,  $p < 0.001$ ). Among the explanatory variables, the standard deviation of temperature (SD\_Temperature) is the only statistically significant predictor ( $\beta = 0.0009$ ,  $p = 0.0414$ ). This result suggests that greater intraannual temperature variability is positively associated with the seasonal deviation in vegetation index, potentially reflecting stronger phenological responses in regions with more distinct seasonal thermal contrasts. Other variables, including SD\_Rainfall, Mean\_Rainfall, and Mean\_Temperature, are not statistically significant at the 0.05 level. However, the negative coefficients of Mean\_Rainfall and Mean\_Temperature may imply a dampening effect of consistently high rainfall or temperature on vegetation seasonality, although the effects are not robustly supported by the data.

#### 5.4. Implications of seasonal bias for downstream applications

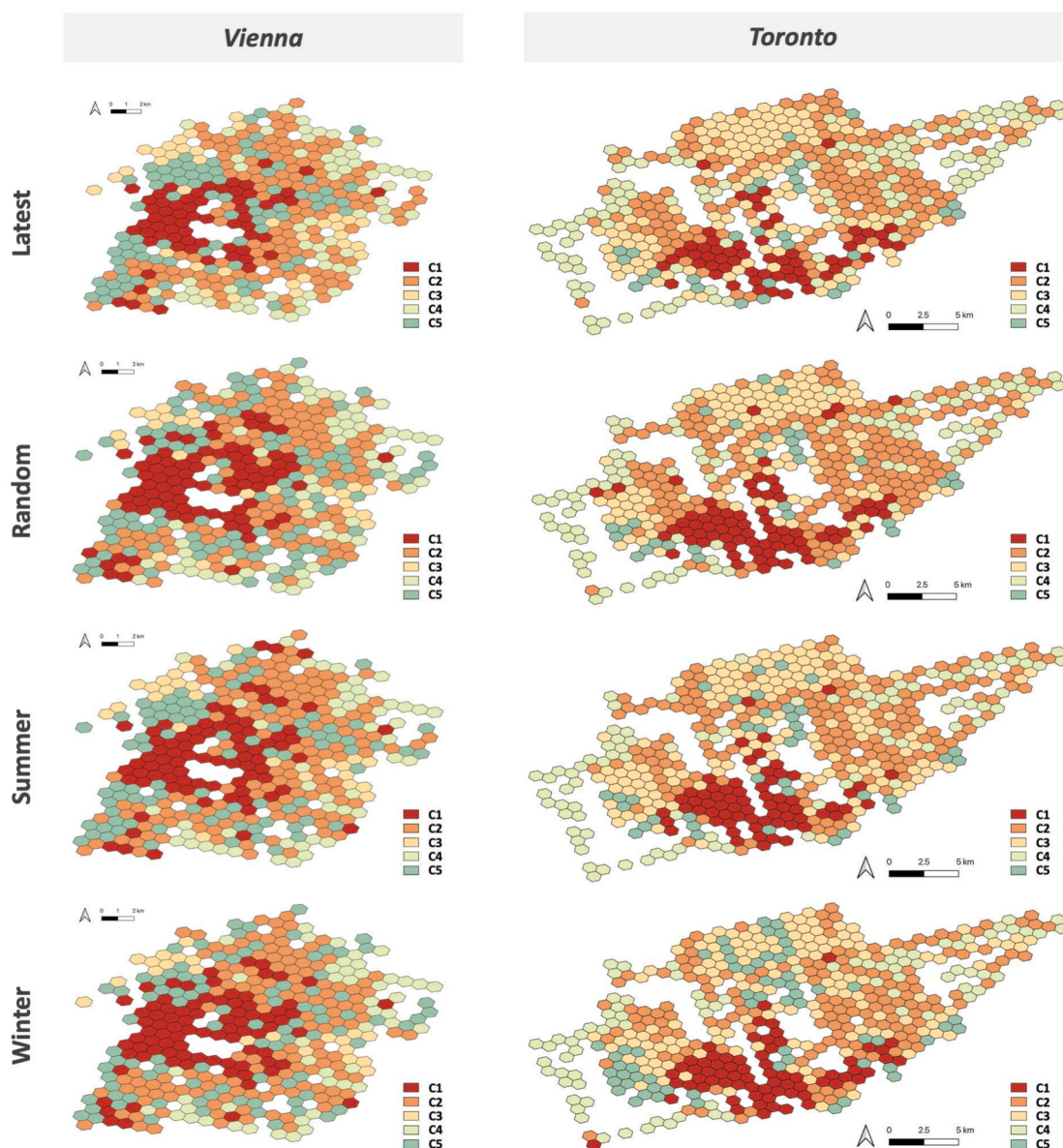
Using Vienna and Toronto as examples, the urban function clustering analysis method of Section 4.2.3 is applied to examine the impact of seasonal bias in SVI on practical applications. In this study, we pre-defined  $k = 5$  for urban functional clustering, based on previous studies (e.g., Liang et al. (2023)) that used a similar approach and the number of clusters to classify urban function or morphology. The five-cluster classification effectively distinguishes major functional structures in a

city, with each cluster exhibiting strong interpretability. Four different data scenarios were constructed for the analysis: latest, random, summer, and winter data. As shown in Fig. 11, the five clusters derived from our k-means analysis (C1–C5) can be broadly assigned to the five categories of urban landscape introduced in Subsection 4.2.3. Based on urban forms in Vienna and Toronto, we infer that C1 corresponds to the downtown commercial core, C2 encompasses mature residential zones, C3 includes peripheral industrial tracts, C4 comprises suburban neighborhoods, and C5 highlights ravine systems and large parks with abundant vegetation.

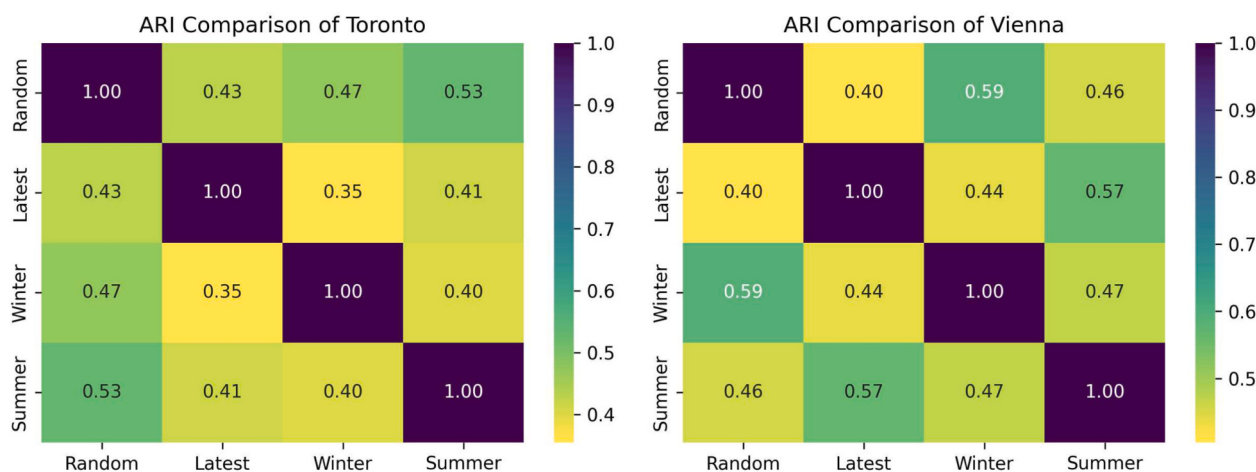
The various data sampling scenarios (latest, random, summer and winter) yield subtle but noticeable shifts in how the five clusters (C1–C5) are distributed throughout Vienna and Toronto. In the latest scenario, for example, C1 (CBD) appears to be more neatly concentrated in central areas, while random sampling scatters a slightly broader range of high-density clusters. In the summer configuration, where vegetation is at its peak, clusters corresponding to greener suburban or natural landscapes (C4 and C5) expand in spatial extent, pushing some mid-density residential zones (C2) into smaller pockets. In contrast, the Winter scenario, which captures less foliage, reveals additional building coverage in areas that otherwise might be classified as suburban, thus redistributing a portion of C4 zones into the higher-BVI categories (C1 and C2). Although the data collection season can alter the boundary lines of each cluster, the fundamental morphological structure remains broadly recognizable.

Fig. 12 presents the ARI comparison results for both cities in the different data scenarios. In Toronto, the ARI values compared to the most recent data are 0.43 for random data, 0.35 for winter data, and 0.41 for summer data, respectively. The ARI values between the random and the summer data is 0.53, indicating the highest similarity between the random and the summer data. In Vienna, the ARI values between the latest data and the random, winter, and summer data are 0.40, 0.44, and 0.57, respectively. The ARI values between random and winter are 0.59, suggesting a greater similarity between random and winter data.

These results indicate that seasonal bias has a significant impact on practical application (urban functional cluster), and different cities may require distinct data combination strategies. In this study, Vienna exhibited the highest ARI value between the random and winter data,



**Fig. 11.** Clustering results under different scenarios.



**Fig. 12.** Heatmap of ARI comparing clustering results across different scenarios.

while Toronto showed the highest ARI between the random and summer data. This phenomenon is likely related to the seasonal characteristics of urban landscapes. In cities where vegetation dominates the summer streetscape, summer data may more accurately represent the city's typical landscape features. In contrast, in cities where vegetation is sparse and winter characteristics are more pronounced, using winter data as representative may be more appropriate. This finding highlights the importance of selecting seasonally appropriate data based on the specific climate and landscape characteristics of each city to ensure the accuracy and consistency of the results of the urban functional area delineation.

## 6. Discussion

### 6.1. Different ways of calculating urban form indicators

Taking the GVI as an example, commonly used calculation methods include semantic segmentation and color thresholding. Color thresholding for the calculation of GVI is a method that identifies green areas in an image by setting specific color value ranges (typically in the RGB or HSV color space) to detect vegetation based on its color (Li et al., 2015). Using Fig. 13 as an example, we illustrate the impact of these different methods on the results. In summer, trees and grass are in their peak growth period, resulting in a larger green vegetation coverage in the images. In contrast, in winter, many trees lose their leaves or rot, and grass can turn yellow or disappear due to low temperatures. Semantic segmentation uses deep learning techniques to perform pixel-by-pixel classification of the image, accurately identifying vegetation areas. This method can maintain relatively stable GVI values even in sparsely vegetated winters. Specifically, the GVI values for summer and winter are 0.245 and 0.232, respectively. However, color thresholding relies on preset color ranges to identify green vegetation, making it more susceptible to seasonal changes. Consequently, the GVI values for summer and winter are 0.237 and 0.046, respectively.

The top 10 cities with the largest GVI discrepancies between summer and winter were selected (as shown in Table 3). We analyze the median and mean of MAPE for these cities. The results show that in cities like Montreal, Denver and Toronto, the median MAPE for the color thresholding method reached 424.563 %, 384.151 %, and 371.822 %, respectively. In contrast, the median MAPE for the semantic segmentation method was 49.882 %, 41.741 %, and 48.092 %, respectively. The discrepancy in MAPE between the two methods exceeded a factor of 10. The results indicate that using different methods to calculate urban indicators from SVI to assess seasonal bias can lead to significant bias, with differences that can exceed tenfold. In comparison, the semantic

**Table 3**

Top 10 cities with the largest differences in GVI between summer and winter by different methods.

City	Color Thresholding		Semantic Segmentation	
	Median MAPE (%)	Mean MAPE (%)	Median MAPE (%)	Mean MAPE (%)
Montreal	424.563	539.333	49.882	90.307
Denver	384.151	548.382	41.741	71.511
Toronto	371.822	538.243	48.092	83.779
Seoul	282.097	399.404	50.458	86.945
Madrid	250.947	416.052	49.281	89.517
Vienna	227.608	374.701	34.645	62.051
London	204.971	362.598	33.902	67.776
Houston	202.780	340.905	29.781	49.909
Tokyo	163.874	288.088	45.177	78.908
Amsterdam	161.060	325.309	31.225	58.225
Istanbul	147.672	236.692	54.791	89.068

segmentation method is better able to handle seasonal changes and reduce deviations when calculating the GVI. Therefore, it is crucial to select the appropriate GVI calculation method based on the experimental objectives and practical requirements.

### 6.2. Implications of seasonal bias in SVI

Seasonal bias in SVI has far-reaching implications for urban greening analysis and broader environmental assessments. Studies often rely on indicators such as the GVI to estimate the coverage of vegetation at street level, a crucial parameter to measure urban greenery and ecological health (Kelly, Davern, Farahani, Higgs, & Maller, 2022; Zhang & Dong, 2021). However, when images are collected during different seasons, particularly in regions with pronounced leaf-on and leaf-off cycles, the same location may exhibit striking discrepancies in GVI values. Furthermore, BVI and SVF, although less sensitive than GVI, also exhibit seasonal bias that can influence the analysis of urban density and sky visibility, respectively.

Beyond greenery, seasonal bias can significantly affect studies on walkability and subjective perceptions of pedestrians of the urban environment. Walkability metrics often incorporate factors such as shade, tree canopy coverage, urban aesthetics, and sidewalk comfort (Ito & Biljecki, 2021). Leafy canopies during warmer seasons can foster more positive user experiences and impressions of safety or aesthetic appeal, while the same sidewalks in winter, strewn with fallen leaves or covered in snow, could appear less inviting and more hazardous. Consequently, a sidewalk audited through SVI in summer might yield a high walkability score, whereas winter images of the same street might lead planners or

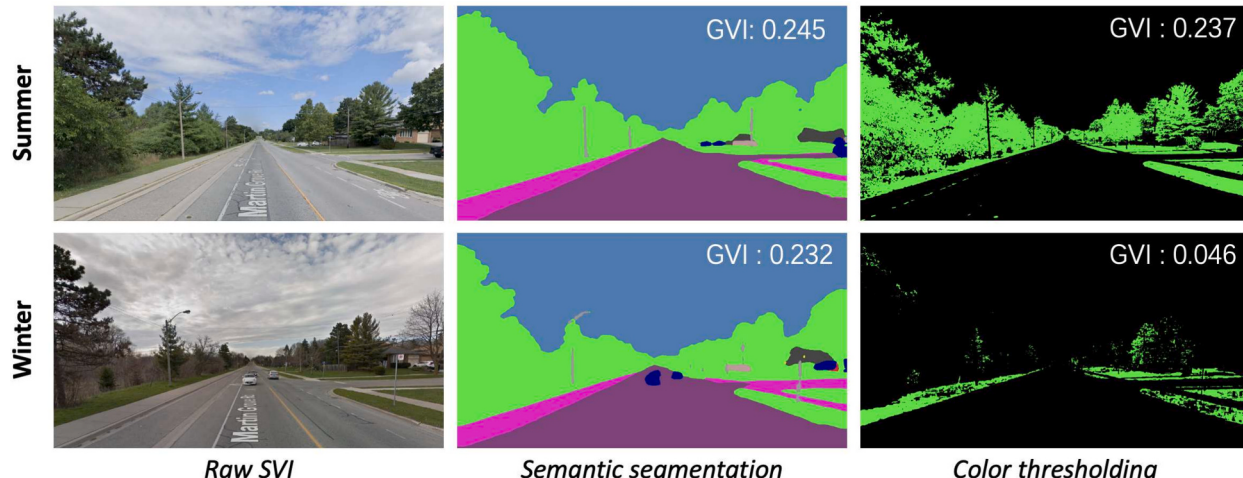


**Fig. 13.** Different methods for calculating the GVI.

researchers to judge it less favorably. Similarly, this bias may extend to studies that focus on street-level economic vitality (Li et al., 2021), as crowded outdoor dining areas or vibrant street markets in summer may appear empty or non-existent in the colder months.

### 6.3. Strategies for mitigating seasonal bias in SVI

One of the most important points about mitigating seasonal bias in SVI is to recognize that not all research contexts require the same level of attention to seasonal effects. Some studies, especially those centered on long-term stable aspects of the built environment (e.g., road layout, building facades, or permanent infrastructure) may tolerate mild seasonal bias without compromising key findings (Chen, Chen, Li, Zhang, & Long, 2023; Liang et al., 2024). Similarly, tropical or subtropical cities with relatively minor seasonal transitions (e.g., consistent foliage throughout the year) may also experience less pronounced seasonal bias (Chen & Biljecki, 2023). However, as soon as a study touches upon features strongly tied to phenology (such as tree canopy coverage), mitigating seasonal bias becomes critical. In terms of analysis of street-level vegetation or detection of time series changes, ignoring the shift between green canopies in summer and barren branches in winter could lead to substantial errors (Li, 2021). The same concern applies to walkability and perception studies that rely heavily on street ambiance, shade availability, and perceived attractiveness, all of which can exhibit dramatic seasonal swings in temperate or continental climates (Wei, Yue, Li, & Gao, 2022).

Further complicating matters is that the degree of seasonal bias is inherently shaped by geographic context and study objectives. Cities near the equator, such as Singapore or Kuala Lumpur, experience minimal temperature and vegetation fluctuations throughout the year, making summer and winter images visually similar. In such settings, comprehensive multiseason sampling may not yield significantly different results, allowing for more flexible or cost-effective data collection without compromising reliability. In contrast, high-latitude cities like Vienna or Toronto undergo dramatic seasonal transitions, such as snow cover, foliage loss, and daylight shifts, making the timing of data acquisition critical for studies involving green coverage, streetscape aesthetics, or pedestrian experience (Liang et al., 2023). As such, a ‘one-size-fits-all’ strategy to control seasonal bias is rarely appropriate. Instead, mitigation efforts should be tailored to the local climate, urban characteristics of interest, and research goals. Depending on the study’s priorities, solutions can range from basic filtering, excluding or flagging images outside a preferred seasonal window (e.g. leaf-on or leaf-off), to more advanced methods such as weighting schemes or sensitivity tests that assess how seasonal fluctuations impact final metrics (e.g., GVI, SVF). If indicators remain robust across seasons, correction may be unnecessary; otherwise, researchers may opt for seasonal averaging or scenario-based representations to clarify differences between warm and cold seasons.

## 7. Conclusion

The increasing use of SVI in urban research has revealed significant challenges related to data consistency and reliability, particularly regarding seasonal bias. Ground-level imagery, captured sporadically in different seasons, can produce inconsistent estimates of urban form indicators such as GVI, BVI, and SVF if sampling time is ignored. To address this problem, we developed a systematic approach that incorporates data filtering, semantic segmentation, and multiscale statistical analyses, examining 689,932 images from 40 cities around the world. By linking an explicit conceptual model of climatic, geographic and data acquisition factors to a two-stage methodological framework, we offered a comprehensive procedure to quantify and understand seasonal bias in SVI.

Through three major research questions, we revealed that (1) RQ1 (extent and spatial distribution of seasonal bias): Even in the same

location, winter and summer SVI can produce significant discrepancies in GVI (e.g., an average MAPE is 54 %), while BVI and SVF also register detectable bias. Statistically, these biases tend to cluster, as evidenced by Moran’s I values exceeding 0.3 in cities such as Toronto and Vienna, underscoring the importance of addressing local heterogeneities in seasonal phenomena. (2) RQ2 (relationship with climate on a global scale): Statistical analyzes indicate a strong correlation between seasonal bias and climatic characteristics. High-latitude, low-rainfall environments manifest more pronounced leaf-on/leaf-off contrasts, producing larger biases in GVI. In contrast, equatorial regions (e.g. Singapore) exhibit smaller fluctuations. These results are further supported by a clustering of k-means of climate variables, revealing distinct patterns of seasonal bias between cities grouped by latitude and temperature variability. (3) RQ3 (practical application errors): we validate the impact of these biases on real-world tasks by examining an urban functional clustering scenario. When data from mismatched seasons were combined, the delineation of land use categories was significantly altered, illustrating the tangible risk of misclassification errors and distorted policy insights if seasonal bias is not adequately addressed.

This study still faces several limitations that open avenues for future research. First, although we carefully controlled the spatial distance among sampled locations (within 18.83 m) and aggregated data to mitigate angular discrepancies, it is challenging to guarantee that SVI from multiple seasons shares identical shooting angles or perspectives. Future studies could adopt image matching techniques (Tian, Chen, & Shah, 2017; Zhu, Yang, & Chen, 2021) or more precise sensor-based localization methods to ensure greater alignment of seasonal images. Second, urban environments are constantly evolving, and even though we restricted our analysis to a 5-year timeframe and focused on relatively mature cities, changes such as infrastructure upgrades, new building construction, and tree removal can alter the built environment in ways unrelated to seasonality. Incorporating remote sensing data (Das & Angadi, 2022; Wang et al., 2020) to detect areas with minimal urban development could help isolate genuinely seasonal bias from those stemming from urban renewal. Third, while this study focuses on city-scale analysis of seasonal bias to ensure cross-regional comparability, future research could explore point-level mechanisms using more granular datasets. Local drivers such as land use types and microclimatic variation can reveal fine-scale heterogeneity in seasonal effects, particularly in temperate regions (Hamid et al., 2023). With access to aligned multi-season images and city-specific contextual data, microscale regression models could offer deeper insights into the relationship between urban microenvironment and seasonal bias of SVI.

## CRediT authorship contribution statement

**Tianhong Zhao:** Writing – review & editing, Writing – original draft, Visualization, Validation, Methodology, Investigation, Funding acquisition, Formal analysis, Data curation, Conceptualization. **Xiucheng Liang:** Writing – review & editing, Writing – original draft, Methodology, Data curation, Conceptualization. **Filip Biljecki:** Writing – review & editing, Writing – original draft, Methodology, Conceptualization. **Wei Tu:** Writing – review & editing, Methodology. **Jinzhou Cao:** Writing – review & editing, Software. **Xiaojiang Li:** Writing – review & editing, Data curation. **Shengao Yi:** Writing – review & editing, Writing – original draft, Project administration, Methodology, Investigation, Data curation, Conceptualization.

## Acknowledgements

This research was supported by the National Natural Science Foundation of China (No. 42401553, No. 42001393); by Natural Science Foundation of Top Talent of SZTU (No. GDRC202415); by Shenzhen Science and Technology Program (No. JYCJ20220530152817039, 20231127180406001); by The Innovation Center of Spatial-temporal Information and Equipment of Smart Cities, MNR (STIEIC-KF202307);

X. Liang acknowledges the NUS Graduate Research Scholarship granted by the National University of Singapore (NUS).

## Appendix A. Supplementary data

Supplementary data to this article can be found online at <https://doi.org/10.1016/j.compenvurbsys.2025.102302>.

## Data availability

Data will be made available on request.

## References

- Anselin, L., Bera, A. K., Florax, R., & Yoon, M. J. (1996). Simple diagnostic tests for spatial dependence. *Regional Science and Urban Economics*, 26, 77–104.
- Biljecki, F., & Ito, K. (2021). Street view imagery in urban analytics and gis: A review. *Landscape and Urban Planning*, 215, Article 104217.
- Biljecki, F., Zhao, T., Liang, X., & Hou, Y. (2023). Sensitivity of measuring the urban form and greenery using street-level imagery: A comparative study of approaches and visual perspectives. *International Journal of Applied Earth Observation and Geoinformation*, 122, Article 103385.
- Cai, H., Li, J., Hu, M., Gan, C., & Han, S. (2023). Efficientvit: Lightweight multi-scale attention for high-resolution dense prediction. In *Proceedings of the IEEE/CVF international conference on computer vision* (pp. 17302–17313).
- Cao, R., Liao, C., Li, Q., Tu, W., Zhu, R., Luo, N., Qiu, G., & Shi, W. (2023). Integrating satellite and street-level images for local climate zone mapping. *International Journal of Applied Earth Observation and Geoinformation*, 119, Article 103323.
- Chen, J., Chen, L., Li, Y., Zhang, W., & Long, Y. (2023). Measuring physical disorder in urban street spaces: A large-scale analysis using street view images and deep learning. *Annals of the American Association of Geographers*, 113, 469–487.
- Chen, J., Zhou, C., & Li, F. (2020). Quantifying the green view indicator for assessing urban greening quality: An analysis based on internet-crawling street view data. *Ecological Indicators*, 113, Article 106192.
- Chen, S., & Biljecki, F. (2023). Automatic assessment of public open spaces using street view imagery. *Cities*, 137, Article 104329.
- Chen, X., Tu, W., Yu, J., Cao, R., Yi, S., & Li, Q. (2024). Lcz-based city-wide solar radiation potential analysis by coupling physical modeling, machine learning, and 3d buildings. *Computers, Environment and Urban Systems*, 113, Article 102176.
- Cheng, L., Chu, S., Zong, W., Li, S., Wu, J., & Li, M. (2017). Use of tencent street view imagery for visual perception of streets. *ISPRS International Journal of Geo-Information*, 6, 265.
- Das, S., & Angadi, D. P. (2022). Land use land cover change detection and monitoring of urban growth using remote sensing and gis techniques: A micro-level study. *GeoJournal*, 87, 2101–2123.
- Dong, X., Yang, R., Ye, Y., Yi, S., Haase, D., & Lausch, A. (2024). Planning for green infrastructure by integrating multi-driver: Ranking priority based on accessibility equity. *Sustainable Cities and Society*, 114, Article 105767.
- Dong, X., Ye, Y., Su, D., Yi, S., Yang, R., Haase, D., & Lausch, A. (2025). Adaptive ranking of specific tree species for targeted green infrastructure intervention in response to urban hazards. *Urban Forestry & Urban Greening*, 128776.
- Fan, Z., Feng, C. C., & Biljecki, F. (2025). Coverage and bias of street view imagery in mapping the urban environment. *Computers Environment and Urban Systems*, 117, 102253.
- Gong, F.-Y., Zeng, Z.-C., Zhang, F., Li, X., Ng, E., & Norford, L. K. (2018). Mapping sky, tree, and building view factors of street canyons in a high-density urban environment. *Building and Environment*, 134, 155–167.
- Hamid, M., Gulzar, A., Dar, F. A., Singh, C., Malik, A. H., Kamili, A. N., & Khuroo, A. A. (2023). Microclimate heterogeneity modulates fine-scale edaphic and vegetation patterns on the himalayan treelines: Implications under climate change. *Agricultural and Forest Meteorology*, 341, Article 109688.
- Han, Y., Zhong, T., Yeh, A. G., Zhong, X., Chen, M., & Lü, G. (2023). Mapping seasonal changes of street greenery using multi-temporal street-view images. *Sustainable Cities and Society*, 92, Article 104498.
- He, J., Zhang, J., Yao, Y., & Li, X. (2023). Extracting human perceptions from street view images for better assessing urban renewal potential. *Cities*, 134, Article 104189.
- Helbich, M., Danish, M., Labib, S., & Ricker, B. (2024). To use or not to use proprietary street view images in (health and place) research? That is the question. *Health and Place*, 87, Article 103244.
- Hou, Y., & Biljecki, F. (2022). A comprehensive framework for evaluating the quality of street view imagery. *International Journal of Applied Earth Observation and Geoinformation*, 115, Article 103094.
- Hou, Y., Quintana, M., Kholiaikov, M., Yap, W., Ouyang, J., Ito, K., ... Biljecki, F. (2024). Global streetscapes—A comprehensive dataset of 10 million street-level images across 688 cities for urban science and analytics. *ISPRS Journal of Photogrammetry and Remote Sensing*, 215, 216–238.
- Ito, K., & Biljecki, F. (2021). Assessing bikeability with street view imagery and computer vision. *Transportation Research Part C Emerging Technologies*, 132, Article 103371.
- Ito, K., Kang, Y., Zhang, Y., Zhang, F., & Biljecki, F. (2024). Understanding urban perception with visual data: A systematic review. *Cities*, 152, Article 105169.
- Juhasz, L., & Hochmair, H. H. (2016). User contribution patterns and completeness evaluation of mapillary, a crowdsourced street level photo service. *Transactions in GIS*, 20, 925–947.
- Kang, J., Körner, M., Wang, Y., Taubenböck, H., & Zhu, X. X. (2018). Building instance classification using street view images. *ISPRS Journal of Photogrammetry and Remote Sensing*, 145, 44–59.
- Kang, Y., Zhang, F., Gao, S., Lin, H., & Liu, Y. (2020). A review of urban physical environment sensing using street view imagery in public health studies. *Annals of GIS*, 26, 261–275.
- Kang, Y., Zhang, F., Peng, W., Gao, S., Rao, J., Duarte, F., & Ratti, C. (2021). Understanding house price appreciation using multi-source big geo-data and machine learning. *Land Use Policy*, 111, Article 104919.
- Kelly, D., Davern, M., Farahani, L., Higgs, C., & Maller, C. (2022). Urban greening for health and wellbeing in low-income communities: A baseline study in Melbourne, Australia. *Cities*, 120, Article 103442.
- Kim, J., & Jang, K. M. (2023). An examination of the spatial coverage and temporal variability of google street view (gsv) images in small- and medium-sized cities: A people-based approach. *Computers, Environment and Urban Systems*, 102, Article 101956.
- Kim, J. H., Lee, S., Hipp, J. R., & Ki, D. (2021). Decoding urban landscapes: Google street view and measurement sensitivity. *Computers, Environment and Urban Systems*, 88, Article 101626.
- Koji, T., Iwata, H., Ishimori, M., Takanashi, H., Yamasaki, Y., & Tsujimoto, H. (2023). Genetic dissection of seasonal changes in a greening plant based on time-series multispectral imaging. *Plants*, 12, 3597.
- Kruse, J., Kang, Y., Liu, Y.-N., Zhang, F., & Gao, S. (2021). Places for play: Understanding human perception of playability in cities using street view images and deep learning. *Computers, Environment and Urban Systems*, 90, Article 101693.
- Li, Q., Cui, C., Liu, F., Wu, Q., Run, Y., & Han, Z. (2021). Multidimensional urban vitality on streets: Spatial patterns and influence factor identification using multisource urban data. *ISPRS International Journal of Geo-Information*, 11, 2.
- Li, S., Ma, S., Tong, D., Jia, Z., Li, P., & Long, Y. (2022). Associations between the quality of street space and the attributes of the built environment using large volumes of street view pictures. *Environment and Planning B: Urban Analytics and City Science*, 49, 1197–1211.
- Li, X. (2021). Examining the spatial distribution and temporal change of the green view index in New York city using google street view images and deep learning. *Environment and Planning B: Urban Analytics and City Science*, 48, 2039–2054.
- Li, X., Zhang, C., Li, W., Ricard, R., Meng, Q., & Zhang, W. (2015). Assessing street-level urban greenery using google street view and a modified green view index. *Urban Forestry & Urban Greening*, 14, 675–685.
- Li, Y., Yabuki, N., & Fukuda, T. (2022). Exploring the association between street built environment and street vitality using deep learning methods. *Sustainable Cities and Society*, 79, Article 103656.
- Li, Z., & Long, Y. (2019). Analysis of the variation in quality of street space in shrinking cities based on dynamic street view picture recognition: A case study of Qiqihar. *Shrinking cities in China: The other facet of urbanization*, 141–155.
- Liang, J., Gong, J., Sun, J., Zhou, J., Li, W., Li, Y., ... Shen, S. (2017). Automatic sky view factor estimation from street view photographs—A big data approach. *Remote Sensing*, 9, 411.
- Liang, X., Chang, J. H., Gao, S., Zhao, T., & Biljecki, F. (2024). Evaluating human perception of building exteriors using street view imagery. *Building and Environment*, 263, Article 111875.
- Liang, X., Zhao, T., & Biljecki, F. (2023). Revealing spatio-temporal evolution of urban visual environments with street view imagery. *Landscape and Urban Planning*, 237, Article 104802.
- Luo, J., Liu, P., Xu, W., Zhao, T., & Biljecki, F. (2025). A perception-powered urban digital twin to support human-centered urban planning and sustainable city development. *Cities*, 156, Article 105473.
- Ma, C., Zhang, Y., Yi, S., & Lu, Y. (2025). Optimizing urban agricultural waste planning and management to enhance sustainability: Strategies for three types of cities. *Sustainable Cities and Society*, 106168.
- Ma, Z. (2023). Deep exploration of street view features for identifying urban vitality: A case study of Qingdao city. *International Journal of Applied Earth Observation and Geoinformation*, 123, Article 103476.
- Mahabir, R., Schuchard, R., Crooks, A., Croitoru, A., & Stefanidis, A. (2020). Crowdsourcing street view imagery: A comparison of mapillary and openstreetcam. *ISPRS International Journal of Geo-Information*, 9, 341.
- Qi, L., Hu, Y., Bu, R., Xiong, Z., Li, B., Zhang, C., Liu, H., & Li, C. (2024). Spatial-temporal patterns and influencing factors of the building green view index: A new approach for quantifying 3d urban greenery visibility. *Sustainable Cities and Society*, 105518.
- Santos, J. M., & Embrechts, M. (2009). On the use of the adjusted rand index as a metric for evaluating supervised classification. In *International conference on artificial neural networks* (pp. 175–184). Springer.
- Shukla, A., & Jain, K. (2019). Critical analysis of spatial-temporal morphological characteristic of urban landscape. *Arabian Journal of Geosciences*, 12, 1–14.
- Tian, Y., Chen, C., & Shah, M. (2017). Cross-view image matching for geo-localization in urban environments. In *Proceedings of the IEEE Conference on Computer Vision and Pattern Recognition* (pp. 3608–3616).
- Tu, W., Chen, D., Cao, R., Xia, J., Zhang, Y., & Li, Q. (2024). Towards sdg 11: Large-scale geographic and demographic characterisation of informal settlements fusing remote sensing, poi, and open geo-data. *ISPRS Journal of Photogrammetry and Remote Sensing*, 217, 199–215.
- Wang, L., Diao, C., Xian, G., Yin, D., Lu, Y., Zou, S., & Erickson, T. A. (2020). A summary of the special issue on remote sensing of land change science with google earth engine.

- Wang, R., Dong, G., Zhou, Y., Du, T., Dong, G.-H., & Helbich, M. (2024). When healthy aging meets vitamin g: Assessing the associations between green space and heart health in older adults using street view and electrocardiography. *Landscape and Urban Planning*, 245, Article 105025.
- Wang, R., Sun, M.-K., Yi, S., Grekousis, G., & Dong, G.-H. (2025). Exploring the associations between street-view green space quantity and quality, and influenza in Guangzhou, China through machine learning and spatial regression: A socio-economic equity perspective. *Environment and Planning B: Urban Analytics and City Science*, 23998083241312272.
- Wang, Z., Ito, K., & Biljecki, F. (2024). Assessing the equity and evolution of urban visual perceptual quality with time series street view imagery. *Cities*, 145, Article 104704.
- Wei, J., Yue, W., Li, M., & Gao, J. (2022). Mapping human perception of urban landscape from street-view images: A deep-learning approach. *International Journal of Applied Earth Observation and Geoinformation*, 112, Article 102886.
- Wu, C., Ye, Y., Gao, F., & Ye, X. (2023). Using street view images to examine the association between human perceptions of locale and urban vitality in Shenzhen, China. *Sustainable Cities and Society*, 88, Article 104291.
- Xia, Y., Yabuki, N., & Fukuda, T. (2021a). Development of a system for assessing the quality of urban street-level greenery using street view images and deep learning. *Urban Forestry & Urban Greening*, 59, Article 126995.
- Xia, Y., Yabuki, N., & Fukuda, T. (2021b). Sky view factor estimation from street view images based on semantic segmentation. *Urban Climate*, 40, Article 100999.
- Xue, F., Li, X., Lu, W., Webster, C. J., Chen, Z., & Lin, L. (2021). Big data-driven pedestrian analytics: Unsupervised clustering and relational query based on tencent street view photographs. *ISPRS International Journal of Geo-Information*, 10, 561.
- Yan, Y., Feng, C.-C., Huang, W., Fan, H., Wang, Y.-C., & Zipf, A. (2020). Volunteered geographic information research in the first decade: A narrative review of selected journal articles in giscience. *International Journal of Geographical Information Science*, 34, 1765–1791.
- Yao, Y., Wang, J., Hong, Y., Qian, C., Guan, Q., Liang, X., Dai, L., & Zhang, J. (2021). Discovering the homogeneous geographic domain of human perceptions from street view images. *Landscape and Urban Planning*, 212, Article 104125.
- Ye, Y., Zeng, W., Shen, Q., Zhang, X., & Lu, Y. (2019). The visual quality of streets: A human-centred continuous measurement based on machine learning algorithms and street view images. *Environment and Planning B: Urban Analytics and City Science*, 46, 1439–1457.
- Yi, S., Li, X., Ma, C., Wang, R., Zhou, Y., Xu, Q., & Zhao, T. (2025). Assessing the differential impact of vegetated and built-up areas on heat exposure environment: A case study of los Angeles. *Building and Environment*, 112538.
- Yi, S., Li, X., Wang, R., Guo, Z., Dong, X., Liu, Y., & Xu, Q. (2024). Interpretable spatial machine learning insights into urban sanitation challenges: A case study of human feces distribution in San Francisco. *Sustainable Cities and Society*, 113, Article 105695.
- Yu, X., Her, Y., Huo, W., Chen, G., & Qi, W. (2022). Spatio-temporal monitoring of urban street-side vegetation greenery using baidu street view images. *Urban Forestry & Urban Greening*, 73, Article 127617.
- Zeng, L., Lu, J., Li, W., & Li, Y. (2018). A fast approach for large-scale sky view factor estimation using street view images. *Building and Environment*, 135, 74–84.
- Zhang, F., Wu, L., Zhu, D., & Liu, Y. (2019). Social sensing from street-level imagery: A case study in learning spatio-temporal urban mobility patterns. *ISPRS Journal of Photogrammetry and Remote Sensing*, 153, 48–58.
- Zhang, M.-J., Dong, R., & Wang, X.-x. (2021). Plants with health risks undermine residents' perceived health status, evaluations and expectations of residential greenery. *Landscape and Urban Planning*, 216, 104236.
- Zhang, Y., Yang, Y., Zhang, L., Zhao, C., Yan, J., Liu, M., & Zhao, L. (2022). Seasonal variation in leaf area index and its impact on the shading effects of vertical green facades in subtropical areas. *Building and Environment*, 225, Article 109629.
- Zhang, Y., Zhang, F., Fang, L., & Chen, N. (2023). Inferring socioeconomic environment from built environment characteristics based street view images: An approach of seq2seq method. *International Journal of Applied Earth Observation and Geoinformation*, 123, Article 103458.
- Zhao, T., Liang, X., Tu, W., Huang, Z., & Biljecki, F. (2023). Sensing urban soundscapes from street view imagery. *Computers, Environment and Urban Systems*, 99, Article 101915.
- Zhu, S., Yang, T., & Chen, C. (2021). Vigor: Cross-view image geo-localization beyond one-to-one retrieval. In *Proceedings of the IEEE/CVF Conference on Computer Vision and Pattern Recognition* (pp. 3640–3649).